

2. EXPLANATORY NOTES¹

Shipboard Scientific Party²

INTRODUCTION

The “Explanatory Notes” chapter is designed to document the primary procedures and methods employed by the various shipboard laboratories during this leg. This information concerns only shipboard methods described in the site reports in the Leg 200 *Initial Reports* volume of the *Proceedings of the Ocean Drilling Program* (ODP). Methods for shore-based analysis of Leg 200 samples and data will be described in the individual scientific contributions to be published in scientific journals and in the *Scientific Results* volume.

Shipboard Scientific Procedures

Numbering of Sites, Holes, Cores, and Samples

Drilling sites are numbered consecutively from the first site drilled by the *Glomar Challenger* in 1968. At a site, multiple holes can be drilled by removing the drill pipe from the seafloor, moving the ship a short distance, and then drilling a new hole. For all ODP drill sites, a letter suffix distinguishes each hole drilled at the same site. The first hole drilled is assigned the site number modified by the suffix “A,” the second hole takes the site number and suffix “B,” and so forth.

The cored interval is measured in meters below seafloor (mbsf). The depth below seafloor is determined by subtracting the water depth estimated from the initial drill pipe measurement, which gives the length of pipe from the rig floor to the seafloor (measured in meters below rig floor [mbrf]), from the total drill pipe measurement. Each cored interval is generally 9.5 to 9.6 m long, which is the length of a core barrel. Coring intervals may be shorter and may not necessarily be adjacent if separated by drilled intervals.

¹Examples of how to reference the whole or part of this volume.

²Shipboard Scientific Party addresses.

A recovered core is divided into 1.5-m sections that are numbered serially from the top. When full recovery is obtained, the sections are numbered from 1 through 7, with the last section possibly being shorter than 1.5 m (Fig. F1); rarely, an unusually long core may require >7 sections. When less than full recovery is obtained, there will be as many sections as needed to accommodate the length of the core recovered. By convention, material recovered from the core catcher of a sedimentary core is placed in a separate section during the core description, labeled core catcher (CC), and placed below the last section recovered in the liner. The core catcher is placed at the top of the cored interval in cases where material is only recovered in the core catcher.

When the recovered core is shorter than the cored interval, the top of the core is equated with the top of the cored interval by convention to achieve consistency in handling analytical data derived from the cores. Samples removed from the cores are designated by distance measured in centimeters from the top of the section to the top and bottom of each sample removed from that section. A full identification number for a sample consists of the following information: leg, site, hole, core number, core type, section number, piece number (for hard rock), and interval in centimeters measured from the top of section. For example, a sample identification of “200-1224D-2R-1, 80–85 cm” would be interpreted as representing a sample removed from the interval between 80 and 85 cm below the top of Section 1, Core 2 (R designates that this core was taken with the rotary core barrel) of Hole 1224D from Leg 200 (Fig. F1).

All ODP core identifiers indicate core type. The following abbreviations are used:

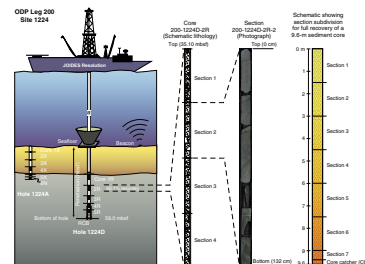
- H = hydraulic piston corer (also referred to as advanced hydraulic piston corer or advanced piston corer [APC]),
- X = extended core barrel (XCB),
- R = rotary core barrel (RCB),
- N = motor-driven core barrel (MDCB), and
- M = miscellaneous material.

Core Handling

Sedimentary Cores

As soon as a core is retrieved on deck, it goes through a sequence of processing steps. Usually, a sample is first taken from the core catcher and given to the paleontological laboratory for an initial age assessment. In the case of Leg 200, no paleontologists were on board, so paleontological samples were not taken. Bob Goll and John Firth of ODP-TAMU (Texas A&M University) performed postcruise analyses of the siliceous (at Site 1223) and calcareous (at Sites 1223 and 1224) nannofossils, respectively. The core is then placed on a long horizontal rack. For safety monitoring, small (~5 cm³) plugs of sediment are also usually taken from the end of one section per core for headspace gas analysis. Gas samples may also be taken by piercing the core liner, typically at voids, and withdrawing gas into a syringe (referred to as vacutainer samples). Because gas hazards in the areas being drilled during Leg 200 were negligible and the sediment cover above basement was thin, no vacutainer samples were collected. Next, the core is marked into section lengths; each section is labeled; and the core is cut into sections. Interstitial water (IW) whole-round samples are then taken as a matter of

F1. Schematic illustrating hole, core, and section labeling, p. 41.



ODP policy (typically on every third core); whole-round samples for microbiology studies may also be taken at this stage if they have been requested. For some of the cores that contain gas, several small holes are drilled into the core liners to allow gas to escape.

Each section is then sealed at the top and bottom by gluing on color-coded plastic caps—blue to identify the top of a section and clear for the bottom. A yellow cap is placed on the section ends from which a whole-round sample has been removed, and the sample code (e.g., IW) is written on the yellow cap. The caps are usually attached to the liner by coating the end liner and the inside rim of the cap with acetone, and then the caps are taped to the liners. The core sections are then carried into the laboratory, where the individual sections are again labeled using an engraver to permanently mark the full designation of the section. The length of the core in each section and the core catcher sample are measured to the nearest centimeter; this information is logged into the ODP Janus database program.

After a core has equilibrated to room temperature, which usually takes ~1–3 hr, each whole-round core section is run through the multi-sensor track (MST), and thermal conductivity measurements are made on soft sediment cores. Whole-round samples for shore-based studies of paleomagnetism, consolidation, shear strength, and other elastic properties may be taken at this stage if they have been requested.

Cores of soft material are split lengthwise into working and archive halves. The softer cores are split with a wire or saw, depending on the degree of induration. Harder cores are split with a band saw or diamond saw. The wire-cut cores are split from bottom to top, so investigators should be aware that older material could have been transported up the core on the split face of each section.

Igneous Cores

Igneous rock cores are handled differently from sediment cores. Once on deck, the core catcher sample is placed at the bottom of the core liner and total core recovery is calculated by pushing the rock pieces together and measuring to the nearest centimeter. The core then is cut into 1.5-m-long sections and transferred into the laboratory.

The contents of each section are transferred into 1.5-m-long sections of split core liner, where the bottom of oriented pieces (i.e., pieces that clearly could not have rotated top to bottom about a horizontal axis in the liner) is marked with a red wax pencil. This is done to ensure that orientation is not lost during the splitting and labeling processes. Important primary features of the cores also are recorded at this time. A plastic spacer is used to separate individual pieces and/or reconstruct contiguous groups of pieces in the core liner. These spacers may represent a substantial interval of no recovery. The length of each section is then recorded and entered into the database as the curated length. The curated length will commonly differ by a few centimeters from that measured on the catwalk. Each piece of core is then split into archive and working halves, with the positions of spacers maintained for both halves. Each piece is numbered sequentially from the top of each section, beginning with number 1; reconstructed groups of pieces are assigned the same number, but they are lettered consecutively. Pieces are labeled only on the outer cylindrical surfaces of the core. If the piece is oriented, an arrow is added to the label pointing to the top of the section.

All Cores

For both sedimentary and igneous cores, the archive half is described visually (see “Core Descriptions,” p. 4). Smear slides are made from small amounts of sediment samples taken from the archive half. Digital images of the archive halves are made on a digital imaging system installed prior to Leg 198. Most archive sections are run through the archive multisensor track (AMST) for color reflectance spectroscopy measurements and susceptibility measurements with a point susceptibility meter and then through the cryogenic magnetometer for magnetic remanence measurements. The archive half then is photographed using black-and-white and color film. Close-up photographs (color and black and white) are taken of particular features for illustrations in the summary of each site, as requested by individual scientists.

The working half of the core is sampled for both shipboard and shore-based laboratory studies. Each extracted sample is logged into the sampling computer database program by the location and the name of the investigator receiving the sample. Records of all removed samples are kept by the curator at ODP. The extracted samples are sealed in plastic vials, cubes, or bags and labeled. Samples are routinely taken for shipboard physical properties, paleomagnetic, thin section, and geochemistry analyses, and microbiological and molecular investigations as described in the sections below.

Following the initial scientific measurements and sampling, both halves of igneous cores are shrink-wrapped in plastic to prevent rock pieces from vibrating out of sequence during transit. The working and archive halves of sedimentary and igneous cores are then put into labeled plastic tubes, sealed, and transferred to cold-storage space aboard the drilling vessel. At the end of Leg 200, the cores were transferred from the ship in refrigerated containers to cold storage at the ODP Gulf Coast Repository at TAMU in College Station, Texas.

CORE DESCRIPTIONS

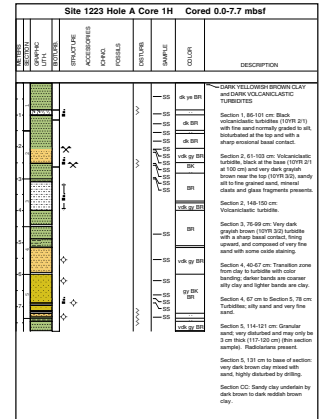
During Leg 200, three general lithologies were described: sediments (at Sites 1223 and 1224), volcanoclastic rocks (at Site 1223), and basalts (at Site 1224). Separate forms were used to describe each lithology.

For sediments, detailed observations of each core were recorded initially by hand on standard ODP visual core description (VCD) forms. These forms provide a summary of the data obtained during shipboard analysis. The sediment VCDs were then entered into the computer using the AppleCORE software. Separate VCDs were custom designed in Adobe Illustrator for the volcanoclastic rocks (volcanoclastic VCDs [V-VCDs]) and the basalts (hard rock VCDs [HR-VCDs]). Both rock types were described on separate forms, and this description was added to the right column of the VCDs. The completed forms were then entered into the computer using Adobe Illustrator. The computerized versions of the visual core descriptions are renamed electronic visual core descriptions (eVCDs) (Fig. F2); V-VCD becomes eV-VCD (Figs. F3, F4), and HR-VCD becomes eHR-VCD (Figs. F5, F6).

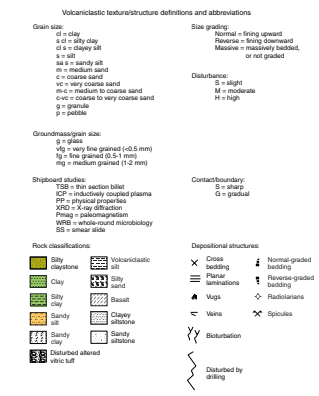
The overall procedures used here are similar to those developed by the scientific parties during ODP Legs 183 (Shipboard Scientific Party, 2000a) and 197 (Shipboard Scientific Party, 2002).

Where appropriate, lithologic names according to the ODP sediment classification scheme (Mazzullo et al., 1988) were used. For volcanoclas-

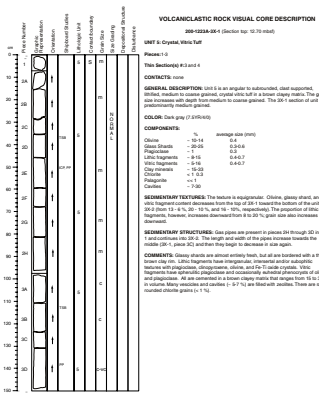
F2. Electronic visual core description form, p. 42.



F3. Electronic volcanoclastic visual core description form key, p. 43.



F4. Electronic volcanoclastic visual core description form, p. 44.



tics, however, we deviated from the standard ODP classification and we adopted a descriptive (nongenetic) terminology similar to that employed during ODP Legs 183 (Shipboard Scientific Party, 2000a) and 197 (Shipboard Scientific Party, 2002).

It is important to remember that the depths recorded for recovered cores may differ from true depths because of curation procedures. The top of the cored material is placed at the top of the cored interval even when recovery is <100%. This is ODP convention. The cored material may in fact have been recovered from deeper in the cored interval.

Sediments

Sediment Classification

Sedimentary structures were described from observations of the split surface of the archive half. Lithologic names follow the ODP sediment classification scheme (Mazzullo et al., 1988). The naming conventions consist of a principal name based on composition, degree of lithification, and texture. For Leg 200, sediment names consist of a principal name (e.g., clay, sand, etc.) and a modifier that precedes the principal name. Minor components that represent between 10% and 25% of the sediment follow the principal name and the word “with” and are listed in order of increasing abundance. Granular sediments are subdivided on the basis of composition and abundance of different grain types estimated from visual examination of the core, smear slides, thin sections, and X-ray diffraction (XRD) analyses. For naming sediments, the Udden-Wentworth grain-size classification scheme (Wentworth, 1922) was used (Fig. F7).

The electronic descriptions for sediments were created using AppleCORE (version 8.1m) software, which generated a simplified, annotated graphic for each core (Fig. F2). Columns on the AppleCORE sheets include depth in core (meters), section number, graphic lithology, bioturbation, structure, disturbance, sample, color, and a description of the core. Features related to sedimentary structures and fossils are plotted on the graphic lithology near the interval in which they are present. The columns on the AppleCORE sheets are discussed below.

Lithology

Sediment lithologies are represented by patterns in the “Graphic Lithology” column (Fig. F8). Limitations of the AppleCORE software result in an inadequate display of thin intervals of interbedded lithologies. These intervals are described in the “Description” column of the AppleCORE sheets.

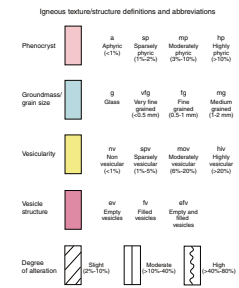
Bioturbation

Bioturbation is represented on the AppleCORE sheets by a symbol in the “Bioturbation” column. Intensity of bioturbation is not depicted by a symbol but is described in the “Description” column.

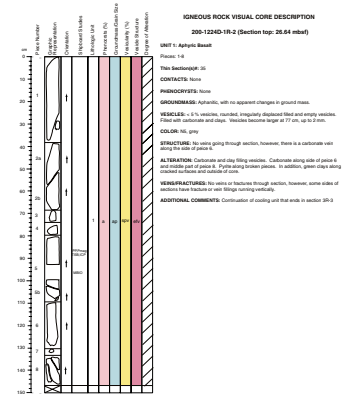
Structures

Sedimentary structures formed by natural processes (i.e., not a result of drilling disturbance) are represented on the AppleCORE sheets with symbols in the “Structure” column. These include varying degrees of grading. A symbol is positioned at the interval in the section where a particular feature is observed (Fig. F8). If the feature extends over an interval, the symbol appears on a vertical line bounded by arrows to denote the extent.

F5. Electronic hard rock visual core description form key, p. 45.



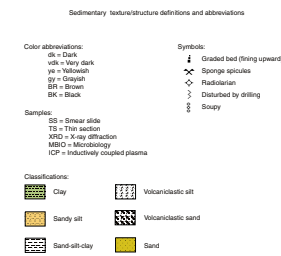
F6. Electronic hard rock visual core description form, p. 46.



F7. Grain-size classification, p. 47.

| Millimeters (mm) | micrometers (µm) | Phi (φ) | Wentworth size class | Rock type |
|------------------|------------------|---------|----------------------|-----------------------|
| 5000 | 5000 | 4.0 | Boulder | Conglomerate/ Breccia |
| 250 | 250 | 5.0 | Cobble | |
| 64 | 64 | 6.0 | Pebble | |
| 4 | 4 | 7.0 | Gravel | |
| 2.00 | 2000 | 8.0 | Sand | Sandstone |
| 1.00 | 1000 | 9.0 | Very coarse sand | |
| 0.50 | 500 | 10.0 | Coarse sand | |
| 0.25 | 250 | 11.0 | Medium sand | |
| 0.125 | 125 | 12.0 | Fine sand | |
| 0.0625 | 62.5 | 13.0 | Very fine sand | |
| 0.03125 | 31.25 | 14.0 | Sand | |
| 0.015625 | 15.625 | 15.0 | Very coarse silt | |
| 0.0078125 | 7.8125 | 16.0 | Medium silt | |
| 0.00390625 | 3.90625 | 17.0 | Fine silt | |
| 0.001953125 | 1.953125 | 18.0 | Very fine silt | Siltstone |
| 0.0009765625 | 0.9765625 | 19.0 | Silt | |
| 0.00048828125 | 0.48828125 | 20.0 | Clay | Claystone |
| 0.000244140625 | 0.244140625 | 21.0 | Very clay | |

F8. AppleCORE sediment key, p. 48.



procedures described in the handbook for shipboard sedimentologists (Mazzullo and Graham, 1988). Identification in terms of general components was undertaken in accordance with Rothwell (1989). Estimates of the proportions of constituents were made using the Comparison Chart for Visual Percentage Estimation (Terry and Chilingar, 1955). In the case of smear slides, however, the percentage had to be corrected to compensate for the degree of dispersion of the grains in the smear slide. Quantitative estimate of grain size and composition are made to the nearest 5% in the tables located in the site chapters.

Smear slides provide only rough estimates of the relative abundances of detrital constituents. This is the result of some fundamental limits:

1. The mineral identification of fine silt- to clay-sized particles is difficult using a petrographic microscope.
2. Sand-sized grains tend to be underestimated because it is difficult to incorporate them in the smear. Care must also be taken to correct for the area taken on the smear by the mounting medium.

Thin Sections of Sediments

Thin sections from the core intervals noted on the VCD forms were examined to complement and refine the hand specimen and smear slide observations. The same terminology that was used for thin section descriptions was used for the VCDs. In sediments, the proportions of lithic, crystal, and vitric components, as well as the finer-grained matrix, were estimated. The textural terms that we used are defined in MacKenzie et al. (1982). Tables summarizing data from thin sections and smear slides are included in the site chapters. These tables include information about the locations of samples in the core and a quantitative estimate of the abundance and composition of different grain sizes and different grain types.

Volcaniclastic Rocks

Volcaniclastic Classification

Unit textures and structures were described from observations of the split surface of both the working and archive cores. A combination of hand samples, smear slides, and thin sections were examined to categorize each unit. Volcaniclastic rocks were classified by designating a principal name with major and minor modifiers. The principal name defines its grain size class (e.g., sand, silt, or clay). Relative proportions of the vitric (glass), crystal (mineral), and lithic (rock fragment) components of the rocks are expressed as major (25%–40%) and minor (10%–25%) modifiers in the name. The major modifiers were placed before the principal name, whereas minor modifiers were placed after the principal name using “with.” For example, a volcaniclastic rock composed of ~2-mm-sized particles, 45% glass, 25% crystals, and 10% lithic fragments, is named crystal vitric tuff with lithic fragments.

We used “volcaniclastic” as a nongenetic term for any fragmental aggregate of volcanic origin and containing >30% volcanic clasts and <70% other types of clastic and/or biogenic material. This definition is broader than that for a pyroclastic deposit. The term “pyroclastic” strictly applies to products of explosive volcanic activity and only includes hydrovolcanic deposits formed by explosive interaction between

magma and water (i.e., hyaloclastite) and nonexplosive quenched fragmentation (i.e., peperite). The term “volcaniclastic” does not imply any active volcanism at the time of deposition; it also includes epiclastic sediments (the volcanic detritus produced by erosion of volcanic rocks).

Unless a pyroclastic origin for the rocks could be determined, we described deposits of volcanic provenance (volcaniclastic) according to the classification scheme for clastic sediments, noting the dominance of volcanic grains. We followed the clastic textural classification of Wentworth (1922) as shown by Boggs (1995) to separate the various volcanic sediments and sedimentary rocks into volcanic gravel (grain size ≥ 2 mm), volcanic sand (2–0.0625 mm), volcanic silt (0.0625–0.0039 mm), and volcanic clay (<0.0039 mm) (Fig. F7). For volcaniclastic sediments, such as those produced by turbidity currents, we did not use the term volcanic ash. Instead we described them as volcaniclastic and named them based on grain size. Indurated units are called lithified, whereas units that are easily broken apart with a fingernail are termed weakly indurated.

Electronic Volcaniclastic Visual Core Descriptions

The electronic descriptions for volcaniclastic rocks were recorded in Adobe Illustrator. The key to the symbols, colors, and other notations used on the eV-VCDs can be seen in Figure F3. The eV-VCD columns, from left to right, are Piece Number, Graphic Representation, Orientation, Shipboard Studies, Lithologic Unit, Contact/Boundary, Grain Size, Size Grading, Depositional Structure, and Disturbance (Fig. F4). These columns are described below.

Piece Number

The left column, “Piece Number,” applies only to the volcaniclastic rocks that are well indurated (e.g., crystal vitric tuffs).

Graphic Representation

A graphic representation of the archive half of the core for the lithified units is shown as a pictorial representation, traced from the digital photo into Adobe Illustrator, in the “Graphic Representation” column. The units that were highly disturbed by drilling or are poorly indurated were not traced from the digital photos; a pattern was used to denote rock type instead.

Orientation

When the orientation of individual pieces was possible, it was indicated on the form by an upward-pointing arrow in the column labeled “Orientation.” A horizontal line across the width of this column denotes a plastic spacer and indicates an interval of no recovery.

Shipboard Studies

Locations of samples selected for shipboard studies are indicated in the column headed “Shipboard Studies” with the following notation: XRD = X-ray diffraction analysis; ICP = inductively coupled plasma-atomic emission spectrometry analysis; TSB = thin section billet; PP = physical properties measurements; MBIO = microbiology sample; and PMAG = paleomagnetic measurements.

Lithologic Unit

The core was subdivided into consecutively numbered lithologic units, under the “Lithologic Unit” column, on the basis of changes in grain size, mineral presence, and abundance.

Contact/Boundary

The “Contact/Boundary” column refers to a relationship between two units that are in contact with one another within a core section. Two types of contacts were listed in this column, sharp and gradational (denoted with S and G, respectively).

Grain Size

The “Grain Size” column is used to describe the size of grains based on Wentworth’s (1922) classification. The following notation is used:

- cl = clay (<0.0039 mm).
- s = silt (0.0039–0.0625 mm).
- vfs = very fine sand (0.0625–0.125 mm).
- fs = fine sand (0.125–0.25 mm).
- m = medium sand (0.25–0.50 mm).
- c = coarse sand (0.50–1.00 mm).
- vc = very coarse sand (1.00–2.00 mm).
- g = granule (2.00–4.00 mm).
- p = pebble (4.00–16.00 mm).
- cl s = clayey silt (a unit of predominantly silt with some clay).
- s cl = silty clay (a unit of predominantly clay with some silt).

For the description of the crystal vitric tuff, we used the following scale for grain size:

- vfg = very fine grained (<0.5 mm).
- fg = fine grained (0.5–1 mm).
- mg = medium grained (1–2 mm).

Size Grading

Size grading refers to the change in grain size within an individual unit. Normal grading refers to the grains becoming finer upward. Reverse grading refers to the grains becoming coarser upward. The word “NORMAL” or “REVERSE” was placed under the “Size Grading” column to denote the type of grading observed.

Depositional Structure

Depositional structure refers to large-scale patterns seen in the sediment and the rocks. It may include laminations, massive rip-up clasts, cross-bedding, cross-laminations, and erosional structures.

Disturbance

The “Disturbance” column is used to denote the amount of disturbance that has taken place in the unit since its deposition. The disturbance was described using the following criteria: no annotation = undisturbed; S = slightly disturbed; M = moderately disturbed; H = highly disturbed.

Written Description of Volcaniclastics

A written core description accompanies the schematic representation of the core sections. This includes leg, site, and hole information in ad-

dition to the headings “Unit,” “Pieces,” “Thin Section(s) #,” “Contacts,” “General Description,” “Color,” “Components,” “Sedimentary Textures,” “Sedimentary Structures,” and “Comments.” These are discussed below.

Leg, Site, and Hole

As with AppleCORE sheets, the leg, site, hole, core type, and section number (e.g., 200-1224D-3R-2), as well as the top and the bottom of the core section measured in meters below seafloor, are located at the top of the written description.

Unit Number and Name

We assigned provisional rock names on the basis of hand specimen observation (hand lens and binocular microscope) and later checked these assignments by examining thin sections.

Pieces

Samples that are lithified are given individual numbers for each piece and these pieces are listed under the “Pieces” heading.

Thin Section(s) #

The number(s) assigned by ODP to the thin section(s) for the lithologic unit described are given under the heading “Thin Section(s) #.”

Contacts

After describing the lithology, we defined unit boundaries. These unit boundaries are listed under “Contacts.” The boundaries often reflect physical changes in the core intervals of the volcanoclastic rocks; changes in vesicularity, alteration, volume fraction, and type of matrix also define lithologic contacts. Where possible, whole-rock chemical analyses by inductively coupled plasma–atomic emission spectrometry analysis (ICP-AES) (see “[Geochemistry](#),” p. 15, in the “Explanatory Notes” chapter) were used to investigate chemical differences between units.

General Description

The “General Description” section was used to give a brief overview of a unit, both macroscopically and microscopically.

Color

“Color” provides a color name and code (for the dry rock surface) according to the Munsell rock color charts (Munsell Color Company, 1994).

Components

The “Components” column includes a list of the principal constituents, their approximate percentages, and their average sizes—determined both petrographically, when thin sections were available, and macroscopically using a binocular microscope for units without thin sections.

Sedimentary Textures

The “Sedimentary Textures” section includes grain size, particle shape (roundness), and grain orientation.

Sedimentary Structures

The “Sedimentary Structures” section includes laminations, cross-bedding, erosion structures, and graded beds.

Comments

Any general descriptions of the unit that were not included under another heading were included under the “Comments” heading. Examples of this include drilling disturbance, freshness of glass shards, and how widespread a particular component is in a unit.

Basalts

Basalt Classification

Basalts cored at Site 1224 are aphyric to sparsely phyric abyssal tholeiites (normal mid-ocean-ridge basalt [N-MORB]) based on chemistry. They include massive flows and holohyaline to hyalopilitic pillows. They were also classified as moderately or strongly differentiated based on chemistry.

Electronic Hard Rock Visual Core Descriptions

Similar to the volcanoclastic rocks, the basalts were described first on paper, then this information was electronically transposed into Adobe Illustrator. The key to the symbols, colors, and other notations used on the eHR-VCDs can be seen in Figure F5. The first five columns of the eHR-VCD form (“Piece Number,” “Graphic Representation,” “Orientation,” “Shipboard Studies,” and “Lithologic Unit”) are identical to the eV-VCD. For a description of these columns, see “[Electronic Volcanoclastic Visual Core Descriptions](#),” p. 8.

The eHR-VCD columns that are different from the eV-VCD include “Phenocrysts (%),” “Groundmass/Grain Size,” “Vesicularity (%),” “Vesicle Structure,” and “Degree of Alteration.” These are described below.

Phenocrysts (%)

The column “Phenocrysts (%)” is used to represent a visual estimation of abundance and variation of phenocrysts throughout the core section using the following notations (Fig. F5):

- A = aphyric (phenocryst content is <1%);
- sp = sparsely phyric (phenocryst content is 1% to 2%);
- mp = moderately phyric (phenocryst content is 3% to 10%); and
- hp = highly phyric (phenocryst content is >10%).

Groundmass/Grain Size

The column “Groundmass/Grain Size” refers to the average size of the groundmass phases:

- g = glass (there are no crystals in the groundmass);
- vfg = very fine grained (average size of the phases is <0.5 mm);
- fg = fine grained (average size of the phases is between 0.5 and 1 mm);
- mg = medium grained (average size of the phases is between 1 and 2 mm); and
- cg = coarse grained (average size of the phases is >2 mm).

If groundmass phases are <0.5 mm in size (vfg), they cannot be seen with the naked eye and the rock is said to be aphanitic (Fig. F5).

Vesicularity (%)

The “Vesicularity (%)” column contains the following abbreviations (Fig. F5):

- nv = nonvesicular (vesicle content is <1%);
- spv or sv = sparsely vesicular (vesicle content is 1% to 5%);
- mov or mv = moderately vesicular (vesicle content is 6% to 20%); and
- hiv or hv = highly vesicular (vesicle content is >20%).

Vesicle Structure

The “Vesicle Structure” column contains the following abbreviations (Fig. F5):

- ev = empty vesicles;
- fv = filled vesicles; and
- efv = empty and filled vesicles.

Degree of Alteration

The “Degree of Alteration” column is used to denote the amount of alteration. The alteration was described using the following: no annotation = unaltered (alteration products form <2% of the rock); diagonal lines = slight (alteration products from 2%–10% of the rock); solid vertical lines = moderate (alteration products form 10% to 40% of the rock); wavy line = high (alteration products form 40% to 80% of the rock) (Fig. F5).

Written Basalt Description

Similar to the eV-VCD, a written core description of the basalts accompanies the schematic representation of the basaltic core sections (eHR-VCD). The description includes the leg, site, and hole information, in addition to the headings “Unit,” “Pieces,” “Thin Sections,” “Contacts,” “Phenocrysts,” “Groundmass,” “Vesicles,” “Color,” “Structure,” “Alteration,” “Veins/Fractures,” and “Additional Comments.” These are discussed below.

Leg, Site, and Hole

As with the AppleCORE sheets and the eV-VCDs, the leg, site, hole, core type, and section number (e.g., 200-1224D-3R-2), as well as the top of the core section measured in meters below seafloor are located at the top of the eHR-VCD description form.

Unit Number and Name

The unit number (consecutive downhole) and the rock name are located next to “Unit.” The provisional rock names were assigned on the basis of hand specimen observations (hand lens and binocular microscope) that were later cross-checked with thin sections and ICP data.

Pieces

“Pieces” refers to the pieces shown in the “Graphic Representation” column with the numbers reported in the “Piece Number” column.

Thin Section(s)#

Where done, “Thin Section(s)#” indicates the number of the thin sections used for the petrographic description of the core.

Contacts

The “Contacts” section includes contact relations and unit boundaries. The unit boundaries were defined based on lithology. The boundaries reflect physical changes in the core (e.g., sequential flows, pillows, or cooling units) that were also observed in the physical properties and downhole measurements. Intervals of sediment, hyaloclastite, and/or changes in vesicularity, chilled margins, alteration, and type of matrix also were used to define lithologic contacts.

Phenocrysts

The “Phenocrysts” entry describes the types of minerals visible with a hand lens or a binocular microscope and their distribution within the unit. The abundance (in volume percentage), range in size (in millimeters), shape, and degree of alteration were determined for each phase.

Groundmass

“Groundmass” includes texture and grain size such as glassy, very fine grained (<0.5 mm), fine grained (0.5–1 mm), medium grained (1–2 mm), or coarse grained (>2 mm) (Fig. F5).

Vesicles

The “Vesicles” section includes the abundance of vesicles (visual estimates of the volume fraction of vesicles were supplemented by observations using a binocular microscope), size, and shape (sphericity/angularity) (Fig. F6). The presence or absence of filling in the vesicles and the type of filling were also noted here.

Color

“Color” includes a color name and code (for the dry rock surface) according to the Munsell rock color charts (Munsell Color Company, 1994).

Structure

“Structure” describes fractures and whether the unit is massive, pillowed, hyaloclastic, banded, or brecciated. The type of alteration mineral lining the fractures was noted. In addition, the presence of alteration adjacent to the fractures and alteration halos was described in this section. We sought to produce an integrated picture of the style of volcanism and environmental setting of each drill site by identifying features that are diagnostic of specific physical processes. Pillowed sequences were inferred using the presence of glassy margins and groundmass grain-size variations. A section was described as massive if there was no evidence for pillows, even though it may be part of a pillowed sequence.

Alteration

“Alteration” describes the degree of alteration as unaltered (<2% of alteration products by volume), slight (2%–10%), moderate (>10%–40%), and high (>40%) (Fig. F5). Changes of alteration through a section or a unit were noted, in addition to the type of alteration material.

Additional Comments

“Additional Comments” describes any general descriptions of the unit that were not included under another heading.

Thin Section Descriptions for Volcaniclastic Rocks and Basalts

Thin sections of volcaniclastic rocks and basalts were examined in order to confirm the visual core descriptions and to better define the textures and relationships among the various constituents of the unit. Moreover, thin section descriptions helped to define the secondary alteration mineralogy and the state of alteration of minerals and glass (where present).

Percentages of individual mineral phases, glass, and alteration products were visually estimated to an accuracy of $\pm 10\%$. A 1000-point mode was determined and was noted in the “Comments” for some thin sections.

Percentages of original paragenesis and of alteration products are given on the detailed thin section description sheets (Fig. F10).

Where possible, a detailed description of the minerals is given. Mineral identifications were made using standard optical mineralogical techniques. In particular, the main aspects considered to identify a mineral phase were shape (under crossed polars [XP] and in plane-polarized light [PP]), habit (XP and PP), color (PP), color (reflected light [RL]), relief (PP), Becke line (PP), interference color (XP), optical sign (conoscopic view with crossed polars [CXP]), determination of optical angle, $2V$ (CXP), and determination of the difference between crystallographic and optical directions (e.g., c^* or a^* ; XP).

The information given in the thin section description sheets includes

1. Modal percent estimate, both visual (semiquantitative) or with point counter (quantitative), based on >1000 points;
2. Size of crystals (smallest, largest, and average; measured along the longest axis in millimeters);
3. Average grain size of the rocks using very fine grained (<0.5 mm), fine grained (0.5–1 mm), medium grained (1–2 mm), and coarse grained (>2 mm);
4. Mineral shape using terms such as prismatic, bladed/lath/shaped, lamellar, tabular, platy, equant, dendritic, skeletal, hollow, and spherulitic;
5. Mineral habit using terms such as anhedral (with no regular edges), euhedral (with crystal faces), and subhedral (with and without crystal faces);
6. Groundmass texture using terms such as intergranular, intersertal, subophitic, holocrystalline, hypocrySTALLINE, hypohyaline, and felty (according to descriptions in MacKenzie et al., 1982);
7. Cavities and vugs (with a regular shape, generally subspherical to spherical) and vesicles (with an irregular shape) percentage, distribution, size (smallest, largest, and average), fillings (also indicating the percentage of fillings) and their relationships; and
8. Veins, describing their width, distribution, and filling.

All basalts cored at Site 1224 are aphyric to sparsely phyrlic.

Representative digital photomicrographs were obtained to better illustrate textures as well as primary and secondary mineralogy.

F10. Thin section description form, p. 50.

GEOCHEMISTRY

ICP-AES Analyses

Chemical analyses of basalts, volcanoclastic rocks, and sedimentary rocks were determined during Leg 200 by ICP-AES. ICP-AES analysis proved difficult during the first half of the leg, mainly because of a problem in recording measurements using the software provided with the equipment. The dysfunction was evidently a flagging procedure in the data acquisition routine. Several protocols were investigated before the problem could be defined and corrected. Even when measurements were finally being recorded properly, however, neither of the two programs on board for calibrating to standards could be used successfully and we were compelled to evaluate the data largely step by step, using averaging and regression functions provided by standard application packages. This was fortunate, for we discovered some difficulties with particular elements that we would not have noticed if we had followed recommended procedures.

We selected representative samples of sedimentary rocks and volcanoclastic rocks (tuffs) from Hole 1223A and basalts from Site 1224 for shipboard ICP-AES analysis. Large whole-rock pieces were first cut with a diamond-impregnated saw blade and ground on a diamond wheel to remove surface contamination. Samples were washed in an ultrasonic bath containing methanol for ~10 min, followed by three consecutive ~10-min washes in an ultrasonic bath containing nanopure deionized water, and then dried for ~12 hr in an oven at 110°C. The cleaned whole-rock samples (~20 cm³) were reduced to fragments <1 cm in diameter by crushing between two disks of Delrin plastic in a hydraulic press and grinding for ~5 min in a Spex 8510 shatterbox with a tungsten carbide barrel. The sample powders were weighed on a Scientech balance and ignited to determine weight loss on ignition (LOI).

Aliquots of 100 ± 2 mg of the ignited whole-rock powders were weighed and mixed with 400 ± 0.4 mg of Li metaborate (LiBO₂) flux that had been preweighed on shore. Standard rock powders and full procedural blanks were included with the unknowns for each sample run. All samples and standards were weighed on the Cahn Electro balance. Weighing errors are conservatively estimated to be ±0.01 mg.

Mixtures of flux and rock powders were fused in Pt-Au crucibles at 1050°C for 10–12 min in a Bead Sampler NT-2100. A total of 10 µL of 0.172-mM aqueous lithium bromide (LiBr) solution was added to the mixture, before fusion, as an antiwetting agent to prevent the cooled bead from sticking to the crucible. Cooled beads were transferred to 125-mL polypropylene bottles and dissolved in 50 mL of 2.3-M HNO₃ by shaking with a Burrell wrist action bottle-shaker for an hour. After digestion of the glass bead, all of the solution was filtered to 0.45 µm into a clean 60-mL widemouthed polypropylene bottle. Next, 2.5 mL of this solution was transferred to a plastic vial and diluted with 17.5 mL of 2.3-M HNO₃ to bring the total volume to 20 mL. The solution-to-sample dilution factor for this procedure is ~4000. Dilutions were conducted using a Brinkmann Instruments dispensette.

Major (Si, Ti, Al, Fe, Mn, Mg, Ca, Na, K, and P) and trace (Zr, Y, Sr, Ba, Ni, Cr, Sc, V, Cu, and Zn) element concentrations of powder samples were determined with the JY2000 Ultrac ICP-AES. The JY2000 sequentially measures characteristic emission intensities (with wavelengths between ~100 and 800 nm). Murray et al. (2000) developed protocols for

dissolution and ICP-AES analysis of rock powders (see also Shipboard Scientific Party, 2001). The hard rock analytical procedure was refined during Leg 197 (Shipboard Scientific Party, 2002). The elements analyzed, the emission lines used, and the specific analytical conditions for each sample run during Leg 200 are provided in Table T1.

The JY2000 plasma was ignited 30 min before each run to allow the instrument to warm up and stabilize. After the warm-up period, a zero-order search was performed to check the mechanical zero of the diffraction grating. After the zero-order search, the mechanical step positions of emission lines were tuned by automatically searching with a 0.002-nm window across each emission peak using the University of Massachusetts Kilauea basalt laboratory standard K-1919, prepared in 2.3-M HNO₃. The only exception is P, which was automatically searched by using a single-element standard. During the initial setup, an emission profile was collected for each peak, using K-1919, to determine peak-to-background intensities and to set the locations of background points for each element. The JY2000 software uses these background locations to calculate the net intensity for each emission line. The photomultiplier voltage was optimized by automatically adjusting the gain for each element using the standard (BHVO-2 or BIR-1) with the highest concentration for that element. Before each run, a profile of K-1919 was collected to assess the performance of the machine from day to day.

All ICP-AES data presented in the site chapter reports were acquired using the Gaussian analytical mode of the Windows 5 JY2000 software. This mode fits a Gaussian curve to a variable number of points across a peak and then integrates to determine the area under the curve. The parameters for each run are given in Table T1. Each unknown sample was run at least twice, nonsequentially, in all sample runs.

A typical ICP-AES run included (1) a set of three certified rock standards (BHVO-2, BIR-1, and BCR-2) (Table T2) run at the beginning, middle, and end of the sample run; (2) as many as 11 unknown samples; (3) a drift-correcting sample (the K-1919 standard) analyzed every fifth sample position, and at the beginning and end of each run; and (4) a blank solution run near the beginning, middle, and end of each run. A 2.3-M HNO₃ wash solution was run for a minimum of 90 s between each of the samples and standards.

Following each sample run, the raw intensities were transferred to an Excel data file, and data reduction was completed using Kaleidagraph. The enhanced plotting functions in Kaleidagraph allowed quick assessment of drift and the repeatability of standards and the blank and identification of occasional discordant measurements. This ensured proper control over standardization and drift correction. Once transferred, a drift correction was then applied to each element and to the blank by linear interpolation between drift-monitoring solutions run before and after a particular batch of samples, assuming that the time between measurements during autosampling was constant. The interpolation was calculated using the lever rule. The drift correction was applied to the blank after noticing for some elements a substantial systematic drift for the blank itself, consistent with the trend of the K-1919 drift monitor. The average of the three drift-corrected procedural blank measurements was then deducted from the drift-corrected intensities of all samples. Following drift correction and blank subtraction, concentrations for each sample were calculated from linear regressions using the average intensity per unit concentration for the three standards measured, each one being measured twice during the run. The blank was also included in the regression with both its intensity and concentration set at

T1. ICP-AES analysis parameters, p. 62.

T2. Typical values for USGS standards analyzed by ICP-AES, p. 63.

zero. This calibration differs from that of previous legs (e.g., Leg 197), in that several standards were used, rather than normalization to a single standard, BHVO-2. The regression technique gave good correlation coefficients (>0.999) for most oxides and trace elements. It also revealed either important discrepancies between standards or problems with sample preparation in the cases of Cu and Zn, which accordingly are not reported in the site chapters.

Estimates of accuracy and precision for major and trace element analyses were based on fits to the regressions for BHVO-2, BIR-1, and BCR-2, the results of which are presented in Table T2. In general, run-to-run relative error by ICP-AES was better than 2% for the major elements. Run-to-run relative error for trace elements was generally $<5\%$. Exceptions typically occurred when the element in question was near the detection limit of the instrument (see Table T1 for instrument detection limits).

X-Ray Diffraction

Secondary minerals (e.g., vein and void fillings) were identified by X-ray diffraction using a Philips PW1729 X-ray diffractometer. Selected samples were taken from the short sections cored at Sites 1223 and 1224. Most samples were taken from small spots in veins or cavity fillings to identify materials with distinctive visual characteristics (the white vug, the green, red, or white mineral lining the vein, etc.). A few were from bulk sediment. The samples were freeze-dried overnight, then crushed to fine grain size using a mortar and pestle, and the powders were mixed in water slurries on glass slides. Upon drying, these were ready for X-ray analysis. Ni-filtered CuK_α radiation was used. The instrument conditions were as follows: 40 kV, 35 mA; goniometer scan from 2° to $70^\circ 2\theta$ (air-dried samples); step size of $0.01^\circ 2\theta$; scan speed at $1.2^\circ 2\theta/\text{min}$; and count time of 0.5 s for each step. In most samples, carbonate minerals were not present, but where they were present we wished to determine their identity. Thus, no samples were decalcified. Also, because of the way the samples were selected, we did not attempt to separate or glycolate clays. MacDiff software (version 4.1.1 PPC, by Rainer Petschick) was used to display diffractograms; identifications are based on multiple peak matches, using the mineral database provided with MacDiff. Diffractograms were peak corrected to match the calcite peak at 3.035 \AA . In the absence of calcite, no peak correction was applied.

PALEOMAGNETISM

Paleomagnetic investigations during Leg 200 consisted mainly of routine remanent magnetization measurements of (1) archive-half sections and (2) discrete samples from the working-half sections, with both being completed before and after alternating-field (AF) demagnetization. In addition, low-field magnetic susceptibility was measured on whole-core sections using the MST device and on archive-half sections using the AMST. To investigate rock magnetic properties, we also conducted thermal demagnetization, anhysteretic remanent magnetization (ARM), and isothermal remanent magnetization (IRM) experiments on some of the discrete samples. To better evaluate the origin and nature of drilling overprints, we measured the remanent magnetization of one whole-round section of sediment, a few long ($>60 \text{ cm}$) whole-round

pieces of basalt, and a few working-half sections before and after demagnetization. Such measurements are only permitted under rare circumstances because they result in partial demagnetization of the entire interval being measured. To preserve the natural remanent magnetization in these intervals, the highest peak field used in demagnetization never exceeded 30 mT.

Instruments and Measurements

Measurements of remanent magnetization were made using an automated pass-through cryogenic magnetometer with direct-current superconducting quantum interference devices (DC SQUIDS) (2-G Enterprises model 760-R). The magnetometer is equipped with an in-line AF demagnetizer (2-G Enterprises model 2G600) capable of producing peak fields of 80 mT with a 200-Hz frequency.

The natural remanent magnetization (NRM) was routinely measured every 1 cm along all archive-half sections before and after AF demagnetization. In interpreting the data, we avoided using the measurements within 5 cm from the ends of each section, although we saved these values for future studies that might wish to deconvolve the remanence signal. AF demagnetizations were applied at multiple demagnetization steps on all sections in steps of 1 to 5 mT up to peak fields of 35 to 70 mT as required to remove drilling overprints and resolve the characteristic remanent magnetizations. The narrow measurement interval, the large number of demagnetization steps, and the high demagnetization levels were selected to allow detailed analysis of vector demagnetization paths. This was possible during Leg 200 because the amount of core recovered was relatively small.

The discrete samples were also measured with the cryogenic magnetometer. Typically samples were demagnetized in steps of 1 to 5 mT from 0 to 80 mT. A few of these samples were further demagnetized at fields up to 150 mT using the DTECH AF demagnetizer (model D2000), with subsequent remanence measurements in the cryogenic magnetometer.

To investigate rock magnetic characteristics of some of the discrete samples, ARM and IRM experiments were conducted and then measured using the cryogenic magnetometer. The DTECH AF demagnetizer was used to impart ARMs to discrete samples, using a 100-mT peak alternating field and a 0.05-mT direct-current (DC) field. The ARMs were imparted along the +z-axis of the samples. We then progressively demagnetized the ARMs at 5-mT increments from 0 to 80 mT using the cryogenic magnetometer. IRMs were imparted to the discrete samples by a DC field generated in the ASC (Analytical Services Company) Impulse Magnetizer (model IM-10). We typically measured the remanence of the discrete samples after imparting (1) an IRM of 1000 mT along the +z-axis, (2) a backfield IRM (BIRM) of 100 mT along the -z-axis, (3) a BIRM of 300 mT along the -z-axis, and (4) an IRM of 1000 mT along the -z-axis. The samples were then stepwise AF demagnetized at 5-mT increments from 0 to 80 mT using the cryogenic magnetometer. In addition, we conducted IRM acquisition experiments and thermal demagnetization of IRMs on a few samples.

Low-field magnetic susceptibility was measured for all whole-core sections as part of the MST measurements (see “**MST Measurements,**” p. 24, in “Physical Properties”). The MST susceptibility meter (a Bartington model MS2 with an MS2C sensor, a coil diameter of 88 mm, and an operating frequency of 0.565 kHz) has a nominal resolution of 2×10^{-6}

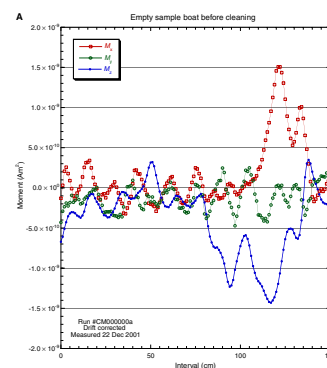
SI (Blum, 1997). Susceptibility was determined at 1- or 2.5-cm intervals using a 1-s integration time and a 4-s period. The “units” option was set on SI units, and the values were stored in the ODP Janus database in raw meter units. To convert to true SI volume susceptibilities, these should be multiplied by 10^{-5} and then multiplied by a correction factor to take into account the volume of material that passed through the susceptibility coils. Except for measurements near the ends of each section, this factor for a standard ODP core is ~ 0.7 (Blum, 1997). No correction was applied for any figures illustrating magnetic susceptibilities in the “Paleomagnetism” sections in the site chapters. Hence, the units are given as raw meter values. Magnetic susceptibility of discrete samples obtained from the working half was measured using a Bartington MS2 susceptibility meter with a dual frequency MS1B sensor. In addition, magnetic susceptibility was measured every 2 cm on the archive halves using the point susceptibility probe (Bartington MS2 susceptibility meter with a MS2F sensor) on the AMST.

Calibration and Instrument Sensitivity

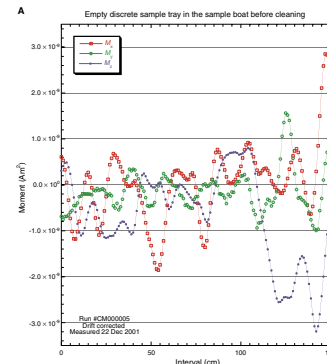
Even though results from the shipboard cryogenic magnetometer have been compared with many other laboratories and shown to give consistent results, it is useful to check the calibration of the magnetometer against a known standard at the beginning of each leg. We used a standard purchased from Geofyzika that is an 8-cm³ cube with an intensity of 7.62 A/m (moment 6.096×10^{-5} Am²). All three axes gave results that agree to better than 1% with this standard. In addition, the automated tray positioning was checked by putting the standard at known positions and measuring the tray. The position indicated by the software was found to be good to ± 1 cm, which is reasonable given the stretch in the pulley system used to move the sample boat.

Based on tests conducted during Leg 186, the background noise level of the magnetometer in the shipboard environment is $\sim 2 \times 10^{-9}$ Am² (Shipboard Scientific Party, 2000b). We repeated tests during Leg 200 for an empty split-core tray (also referred to as the sample boat) and for the tray that holds discrete samples (Figs. F11, F12). Several discrete trays are available for use, but we only used the tray provided by 2-G Enterprises. This tray is 150 cm long and has holders for samples with 2 cm \times 2 cm bases at 10, 30, 50, 70, 90, 110, and 130 cm and holders for samples with 2.6 cm \times 2.6 cm bases at 20, 40, 60, 80, 100, 120, and 140 cm. It sits in the sample boat when used. We first measured the sample boat before and after cleaning it (Fig. F11A, F11B), where the cleaning consisted of spraying the boat with window cleaner and wiping it clean followed by AF demagnetization at 60 mT. The noise is noticeably reduced by cleaning, although in both cases it is less than $\pm 2 \times 10^{-9}$ Am². We also repeated the cleaned sample boat measurement several times over a 2-day period and got very similar results for all three axes, indicating that the signal shown in Figure F11B is not random noise of the instrument but a coherent signal related to the cleaned sample boat. When the discrete sample tray is placed in the sample boat, the noise level increases. It is slightly greater than $\pm 2 \times 10^{-9}$ Am² before cleaning (Fig. F12A) and slightly less after cleaning (Fig. F12B). The clean discrete sample tray measurement was repeated a few days later with the addition of empty plastic cubes in the tray, resulting in noise that exceeded $\pm 3 \times 10^{-9}$ Am² (Fig. F12C). Thus, the practical noise level is related to the magnetization of the plastic cubes (for discrete samples) and to dirt on the sample boat or tray. Some of this noise can be re-

F11. Magnetic moment measured for an empty sample boat, p. 51.



F12. Magnetic moment measured for an empty discrete sample tray sitting within the sample boat, p. 53.



moved by subtracting the tray magnetization from sample measurements, but again dirt on the tray can accumulate. Even with diligence, it is difficult to keep the trays clean given the amount of core material measured during a typical leg. For long core measurements, it is not practical to clean and remeasure the empty tray before each new sample. Thus, the correction for the tray magnetization may not improve the accuracy of the measurements significantly. Furthermore, the split-core sections are in a plastic core liner that has been stored in dusty conditions prior to coring and that resides in a metal core barrel just prior to core collection. Therefore, the noise associated with the core liners will likely be several times greater than the noise associated with the sample boat.

We conclude that under favorable conditions the noise level will be $\sim \pm 2 \times 10^{-9}$ Am². For a split core, given the large volume of core material within the sensing region of the magnetometer, which is ~ 100 cm³, the minimum measurable remanent intensities will be greater than $\sim 2 \times 10^{-5}$ A/m. For discrete samples, which typically have volumes of 6–10 cm³, the minimum measurable remanent intensities are greater than $\sim 4 \times 10^{-4}$ A/m. Results from measurements during several cruises indicate that accurate measurements are likely to be obtained when both split-core and discrete samples have intensities about two to five times higher than the background noise level, or when they have intensities greater than $\sim 10^{-4}$ A/m and 10^{-3} A/m, respectively.

Core Orientation

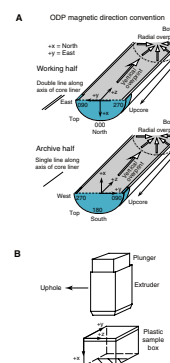
The standard ODP paleomagnetic coordinate system was used. In this system, +x represents the vertical upward from the split-core surface of archive halves, +y is left along split-core surface when looking upcore, and +z is downcore (Fig. F13A).

Given the limited APC coring that was conducted, we did not have the opportunity to use the Tensor tool for azimuthal core orientation during Leg 200. For hard rocks it is possible to combine images of the exterior of the core with images of the borehole wall from the Formation MicroScanner (FMS) logging tool. To allow for this possibility, the exterior of all basalt cores were scanned with the new digital camera system. We first marked a line on the top of each core piece indicating where the core would be split into archive and working halves. The whole-core pieces were scanned in this orientation, and then each piece was rotated counterclockwise 90° about the -z-axis and scanned. The process was repeated for 180° and 270° rotations, resulting in four images of each piece, with the hope that the four images could be correlated with the four images provided by the sensor pads on the FMS.

Sampling Methods and Orientations for Discrete Samples

Oriented discrete samples were taken from the working half of each section (typically one or two per section for shipboard analyses) using plastic cubes with a 2 cm × 2 cm × 2 cm exterior dimension and an aluminum extruder. The interior volume of a cube is ~ 7 cm³. Each plastic cube has an arrow on the bottom face. The sediment is collected in the extruder with a 2 cm × 2 cm cross-section opening (Fig. F13B). Usually a few millimeters of sediment is extruded and removed from the bottom of the extruder with a spatula, leaving a flat surface of sediment and

F13. ODP paleomagnetic coordinate system, p. 56.



just enough sediment in the extruder to fill the plastic cube. The sediment is then carefully extruded into the plastic cube. An orientation mark on the extruder aids in ensuring the upcore orientation of the sample is maintained, and a mark on the plunger in the extruder aids in ensuring that enough sediment is collected to fill the plastic cube.

In lithified intervals, we drew an arrow on the split-core face pointing uphole and used the rock saw to cut the sample. When measuring the sample, we placed the side with the arrow down in the tray with the arrow pointing along the $-z$ -axis, or uphole, direction. This makes the discrete sample orientation the same as that of the archive halves, which allows for a more direct comparison of the discrete sample results with archive-half results.

We also cut small chips or cubes (~ 0.5 – 1.5 cm³) and drilled ~ 1.1 -cm³ minicores (1.2 cm diameter and ~ 1 cm long) from hard rock cores to assess differences in the drilling overprint from the periphery of the core to its interior. These were oriented with an arrow pointing uphole and drawn along the split-core face or along the face closest to and parallel (or tangent for cylinders drilled along the z -axis) with the split-core face. These were measured in the magnetometer with the arrow pointing along the $-z$ -axis, or uphole, and with the side with the arrow facing up or down, as noted for specific tests. In all cases, the arrow on the discrete samples points upcore.

Magnetic Overprints

Several types of secondary magnetization were acquired during coring, which sometimes hampered magnetostratigraphic and paleomagnetic interpretation. The most common was a steep downward-pointing overprint attributed to the drill string. For the Leg 200 cores, we also observed a bias for 0° declinations, which has been observed during many previous cruises and has been interpreted as a radially inward overprint (Fig. F13A). We sampled the periphery and interior of core pieces to better document the nature of the overprints for different lithologies cored at the two sites. Other overprints related to diagenesis or tectonic deformation were observed. Details of these and other magnetic complexities are presented in the site chapters.

Magnetostratigraphy

Where AF demagnetization successfully isolated the characteristic component of remanence, paleomagnetic inclinations were used to define polarity zones. Ages for reversals are from the revised Cenozoic timescale of Cande and Kent (1995).

MICROBIOLOGY

The primary microbiology objective for Leg 200 was to explore the composition of the microbial communities associated with deep marine sediments and the pore space as well as pore water fluids in the oceanic crust. To address these topics, a multiphasic approach comprising cultivation-based and culture-independent methods was conducted. For that purpose, sediment and rock samples were collected, and the presence of microorganisms was determined by fluorescent total cell count staining techniques (Live/Dead staining, deoxyribonucleic acid [DNA]-binding fluorochromes like 4',6-diamidino-2'-phenylindole-dihydro-

chloride [DAPI], SYBR Green, and SYTO 62) and by fluorescent in situ hybridization (FISH) using domain- and group-specific oligonucleotide probes. The most probable number (MPN) was estimated for sulfate-reducing bacteria and fermentative bacteria. In addition, enrichment cultures of microorganisms putatively inhabiting these environments were established under aerobic and anaerobic conditions. Further samples were taken in order to extract the total DNA of the microbial communities for postcruise analysis of microbial diversity and to assess proxies of the microbial activity by the determination of different biomarkers including eubacterial phospholipid fatty acids and other lipids.

Sediments

Sampling

Whole-round samples were cut from the cores for microbiological investigations. The cores were cut and capped on the catwalk and immediately transported to the microbiology laboratory. The surface of the samples was removed with sterile spatulas and spoons, and subsamples ranging from 1 to 5 g were taken under sterile conditions.

Microbial Abundance

Sediment samples (3–5 g) were taken from the inner part of the whole-round sample, suspended in 1× PBS (130-mM sodium chloride, 10-mM sodium phosphate buffer, pH 7.2 [Dulbecco's phosphate-buffered saline]) and fixed with 0.2- μ m filtered formaldehyde solution (2% final concentration) for at least 4 hr at 4°C. Sediment samples were centrifuged at 5000 rpm for 20 min (Marathon 21K; Fisher Scientific), thoroughly washed twice with 1× PBS and stored in a 1:1 mixture of 1× PBS and 99.9% ethanol at 4°C. To determine the microbial abundance, fixed samples were stained with DAPI, SYBR Green, or SYTO 62. To determine the amount of living bacteria, aliquots of the samples (1 mL) were filtered onto black, 13-mm-diameter polycarbonate filters (0.2- μ m pore size) in a filtration tower, mounted on microscope slides with a drop of nonfluorescent mounting oil, and examined using the Live/Dead staining kit and epifluorescence microscopy.

Electron Microscopy

For shore-based scanning and transmission electron microscopy analyses (SEM and TEM, respectively), sediment samples were fixed with freshly prepared buffered glutaraldehyde solution (2% final concentration), washed twice with 1× PBS and stored in 1× PBS at 4°C.

Cultivation

Subsamples from the suspended sediments were plated onto solid media plates of different trophic levels and incubated under aerobic and anaerobic conditions, respectively. Enrichment cultures selective for sulfate-reducing, fermentative, and facultative anaerobic bacteria were established. The cultures were incubated at 4°C and room temperature. For further cultivation, 800- μ L aliquots were preserved and frozen immediately after sampling at -76°C using the commercial Mikrobank system.

Fluorescence In Situ Hybridization

To study the distribution and phylogenetic affiliations from the sediment associated bacteria in more detail, FISH was performed by applying probes of different phylogenetic levels on the bacteria within the suspended formaldehyde-fixed sediments. Fixed samples were also transported to the University of Göttingen for embedding and analyzing thin sections of the sediments with the FISH technique.

DNA Extraction

Samples obtained from the native sediment as well as of the sediment suspensions were taken and frozen immediately at -76°C . These frozen samples were transported to the University of Göttingen for further postcruise DNA extraction and DNA-based analysis of the microbial diversity and in-depth phylogenetical characterization.

Biomarker Analysis

Subsamples of the sediments were frozen immediately at -76°C in sterile aluminum foil and were transported to the University of Göttingen for extraction and determination of different biomarkers including eubacterial phospholipid fatty acids and other lipids.

Igneous Rocks

Sampling

Whole-round core samples were collected on the catwalk from the end of an unsplit core liner or in the core splitting room immediately after the core liner was split, or a minicore was taken. Cores were handled with ethanol-treated latex gloves, and the surfaces of the cores were disinfected with isopropanol. The cores were subsequently crushed, and inner parts were ground under aseptic conditions and suspended in $1\times$ PBS. The suspensions were used for the inoculation of the agar plates and enrichment cultures. Subsamples for DNA extraction were obtained as described below.

Microbial Abundance

Small pieces of crushed rock (3–6 mm in diameter) as well as ground rock material were fixed with formaldehyde and glutaraldehyde solutions as described above. Samples were stained with different DNA staining dyes. To assess the inherent autofluorescence of the samples, untreated control rock samples were investigated.

Cultivation

For the establishment of enrichment cultures as described above, small pieces obtained from the inner parts of crushed rocks as well as suspended ground material were used as inocula. Suspended ground material was additionally plated onto the agar plates.

Fluorescence In Situ Hybridization

Whole-rock pieces split from the interior part of the cores were fixed as described above and stored for further embedding and thin section-

ing at the University of Göttingen. FISH will also be performed on thin sections of the basaltic rock samples.

Electron Microscopy

For shore-based SEM and TEM analyses, samples were fixed with glutaraldehyde as described above. Thin sections will be made at the University of Göttingen.

DNA Extraction

Whole-rock pieces split from the interior part of the cores were frozen at -76°C in sterile aluminum foil immediately after sampling for shore-based DNA extraction and analysis.

Biomarker Analysis

Large pieces of crushed rocks were frozen at -76°C in sterile aluminum foil immediately after sampling and were transported to the University of Göttingen for the investigation of different biomarkers.

PHYSICAL PROPERTIES

Shipboard measurements of physical properties can be used to provide an initial look at variations in the recovered core material, which may be used to characterize lithologic units, correlate with downhole geophysical logging data, and interpret seismic reflection data. After the cores had attained room temperature, nondestructive tests of the whole-round (unsplit) core sections were made with the MST. After splitting the cores, additional measurements were made of *P*-wave velocity on split cores of soft sediments and on discrete samples of hard rock. Bulk density, grain density, porosity, and water content were calculated from moisture and density measurements on discrete samples. Thermal conductivity measurements were also made on whole sediment cores and split hard rock cores. The instruments and apparatus used during Leg 200 are discussed in Blum (1997) and are outlined below.

MST Measurements

The MST consists of four physical property sensors on an automated track that measures magnetic susceptibility, bulk density, compressional wave velocity, and natural gamma ray emissions on whole-round core sections. During Leg 200, magnetic susceptibility, gamma ray attenuation (GRA) bulk density, and natural gamma ray were measured on both soft sediment cores and hard rock cores; compressional wave velocities were measured using the *P*-wave logger (PWL) on APC cores.

Magnetic Susceptibility

Magnetic susceptibility was measured on all sections at 1- or 2.5-cm intervals using the 1.0 range (1-s integration time) on the Bartington meter (model MS2C), which has an 88-mm coil diameter. The magnetic susceptibility data aid in detecting variations in magnetic properties caused by lithologic changes or alteration. The quality of the magnetic susceptibility measurement is somewhat limited in sedimentary cores if

they are disturbed. However, general trends may still be useful for correlation with geophysical logging data. The units for the stored data and instrument sensitivity are given in "[Paleomagnetism](#)," p. 17.

Gamma Ray Attenuation

GRA measurements estimate bulk densities on unsplit core sections using a sampling period of 5 s every 1 or 2.5 cm. GRA data are most reliable in undisturbed cores and can often be directly correlated with the downhole density logs. In disturbed soft sediment cores, GRA density would be expected to give values lower than the true values for undisturbed sediments.

Natural Gamma Ray Emissions

Natural gamma ray (NGR) emissions result from the decay of radioactive atoms and were measured in the laboratory by scintillation detectors as described by Hoppie et al. (1994). During Leg 200, NGR measurements were made at intervals of 10 cm for a period of 20 s on soft sediment and for a period of 60 s on hard rock cores. Results were output in counts per second, which can then be compared qualitatively with the downhole logging data. The NGR was calibrated using a thorium and potassium source.

Thermal Conductivity

Thermal conductivity was measured on unconsolidated sediment and rock samples using the TK04 system as described by Blum (1997). These measurements are used, along with in situ temperature measurements, to estimate heat flow. The system uses a single-needle probe (Von Herzen and Maxwell, 1959) heated continuously in full-space mode for soft sediments and in half-space configuration for hard rock samples (Vacquier, 1985). For full-core soft sediment sections, a hole was drilled in the outer core liner and a 2-mm temperature probe was inserted into the working half of the core section. For hard rock samples, a half-space needle probe was secured on ~5-cm split-core sections that had been immersed in a water bath for at least 15 min. The thermal conductivity measurement for each sample was the average of three repeat measurements for the full-space method and of four repeat measurements for the half-space method. All results are in units of watts per meter degree Kelvin.

Moisture and Density Properties

Samples of ~10 cm³ for sediments and <10 cm³ for hard rock samples were collected at a frequency of one per section to allow for determination of moisture and density. Samples were taken from undisturbed parts of the core if possible. Wet sediment mass was measured immediately after the samples were collected. Dry sediment mass and dry sediment volume were determined after the samples had been dried in a convection oven for 24 hr at a temperature of 100°–110°C. Wet and dry masses were measured with two Scientech 202 electronic balances that compensate for the ship's motion; dry volume was determined with a helium-displacement Quantachrome penta-pycnometer. For hard rock sections, the samples were soaked in seawater for 24 hr, then moisture

and density properties were measured using the same procedure as for the sediment sections.

Grain density, moisture content, bulk density, and porosity were calculated from wet and dry mass and dry volume as discussed by Blum (1997), who also gives values of seawater density, seawater salt density, and seawater salinity used in the calculation. Grain density (ρ_g) can be calculated from the measurements of dry mass (M_d) and dry volume (V_d). Both of these values need to be corrected to take into account the salt content of the pore fluid,

$$\rho_g = (M_d - M_s)/(V_d - [M_s/\rho_s]),$$

where ρ_s is salt density (2.257 g/cm³), and M_s is the mass of salt in the pore fluid.

The uncorrected water mass is taken as the difference between the total (water saturated) mass (M_t) and the dry mass (M_d). The measured wet and dry masses are corrected for salt content using a pore water salinity (r) of 0.35% (Boyce, 1976). The wet and dry moisture contents are calculated by

$$W_d (\% \text{ dry mass}) = [(M_t - M_d)/(M_d - rM_t)] \cdot 100 \text{ and}$$

$$W_w (\% \text{ wet mass}) = [(M_t - M_d)/(-rM_t)] \cdot 100.$$

The bulk density (ρ_b) is the density of the saturated sample,

$$\rho_b = M_t/V_t$$

where V_t is the total sample volume.

Porosity (Φ) can be calculated from fluid density, grain density, and bulk density of the sample and is the ratio of pore water volume to total volume,

$$\Phi = [(\rho_g - \rho_b)/(\rho_g - \rho_w)] \cdot 100,$$

where ρ_w is the density of the pore fluid (seawater).

Velocity Determinations

For sediment sections, velocity determinations were made by the PWS3 contact probe system. Using this system, P -wave velocities on the x-, y-, and z- directions were measured on minicubes that were also used for shipboard paleomagnetic measurements.

DOWNHOLE MEASUREMENTS

Downhole logging began in the 1920s as “electrical coring” (Schlumberger et al., 1934), which measured the spontaneous potential (SP) between the surface and the sonde at depth. It now encompasses a wide range of sensors. It is a method of measurements performed in a drill hole to determine the in situ physical, chemical, and structural properties of formations penetrated by the hole. The borehole data so obtained are called logs, and they can be acquired after the hole is drilled (wireline logging) or while/after drilling (logging while drilling [LWD])

or during drilling (measurement while drilling). Wireline logging is most effective in stable formations where the hole is nearly vertical, whereas LWD can be performed while drilling where formations are unstable or after drilling where the hole is deviated far from the vertical. Wireline logging was used during Leg 200.

The combinations of wireline logs on the *JOIDES Resolution* are collected at a speed of 250–300 m/hr, using a variety of instruments that make continuous in situ measurements as a function of depth. The sampling interval of log data ranges from 2.5 mm to 15 cm in depth. Logs are useful for relating the borehole lithostratigraphy with regional geophysical studies. Where core recovery is incomplete or disturbed, log data may provide the only means to characterize the drilled formations. After processing, logs are typically displayed as curves or images of physical and chemical properties of the formations intersected by the borehole. Image logs, in particular, serve to illustrate the physical shape and state of the hole and the character of the formations penetrated. Log data have been used for an ever-growing number and range of applications, such as characterizing formation fluids and measuring the in situ temperature and stress conditions.

Log data quality is largely determined by the state of the borehole wall and individual logging tools. There is also a small but significant difference between drill pipe depth and logging depth that should be taken into account when the logs are used for correlation with core and log measurements. In addition, logs from different wireline tool strings may have slight depth mismatches. Therefore, after data acquisition, basic hole-condition correction and depth match are generally required. With further processing, log data are combined with core and seismic data to achieve integrated characterization, analysis, and interpretation of both formation fluids and subsurface environments.

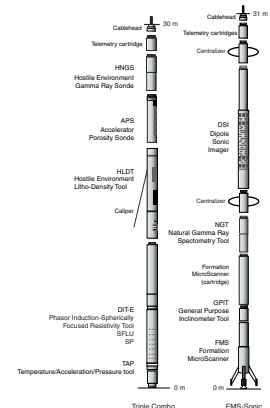
Logging Tool Strings and Operations

During Leg 200, Hole 1224F was drilled, cored, and logged. The logs were acquired using a variety of Schlumberger and Lamont-Doherty Earth Observatory Borehole Research Group (LDEO-BRG) logging tools that are combined into several “tool strings.” Three wireline tool strings were used:

1. The triple combination (triple combo) tool string (resistivity, density, and porosity) (see Fig. F14) consists of the Accelerator Porosity Sonde (APS), the Hostile Environment Litho-Density Tool (HLDT), and the Phasor Dual Induction–Spherically Focused Resistivity Tool (DIT-E). The Hostile Environment Gamma Ray Sonde (HNGS) is included at the top of the string, and the LDEO-BRG Temperature/Acceleration/Pressure (TAP) tool is at the bottom.
2. The FMS/sonic tool string (Fig. F14) consists of the FMS, the General Purpose Inclinerometer Tool (GPIT), and the Dipole Sonic Imager (DSI). The Natural Gamma Ray Spectrometry Tool (NGT) is also included in this tool string.
3. The three-component Well Seismic Tool (WST-3) (Fig. F14) is used to correlate borehole measurements with surface seismic data.

Each tool string contains a telemetry cartridge facilitating communication from the tools along a double-armored seven-conductor wireline

F14. Schematic illustration of tool string configurations, p. 57.



cable to the Schlumberger Minimum Configuration Maxis (MCM) computer van on the drillship. The 9000-m-long logging cable connects the MCM to the tool string through the logging winch and LDEO-BRG wireline heave compensator (WHC).

The WHC is employed to minimize the effect of the ship's heave on the tool position in the borehole. The logging winch is located aft of the pipe racker. The 160-m-long logging cable fairlead runs from the winch forward to the drill floor, through a sheave back to the heave compensator located alongside the logging winch, then forward to another sheave on the rig floor, up to the crown block on the top of the derrick, and then down into the drill string. As the ship heaves in the swell, an accelerometer located near the ship's center of gravity measures the movement and feeds the data, in real time, to the WHC. The WHC responds to the ship's heave by hydraulically moving the compensator sheave to decouple the movement of the ship from the desired movement of the tool string in the borehole (Goldberg, 1990).

In preparation for logging, the boreholes are usually flushed of debris by circulating a "pill" of viscous drilling fluid (sepiolite mud mixed with seawater; approximate weight = 8.8 lb/gal or 1.11 g/cm³) through the drill pipe to the bottom of the hole. The bottom-hole assembly (BHA) is pulled up to a depth between 50 and 100 mbsf then run down to the bottom of the hole again to ream borehole irregularities. The hole is subsequently filled with more sepiolite mud, and the pipe is raised to ~50–70 mbsf and kept there to prevent hole collapse during logging. During Leg 200, the tool strings were lowered downhole during sequential runs. During each logging run, incoming data are recorded and monitored in real time on the MCM computer. The tool strings are then pulled up at constant speed to provide continuous measurements as a function of depth of several properties simultaneously. After the logs are acquired, the data are transferred to the downhole measurements laboratory (DHML) and also to LDEO-BRG for processing using a high-speed satellite data link. The TAP tool is usually deployed as a memory tool. Extraction and processing of the TAP tool data are done in the DHML using a specialized acquisition system.

Tool Measurement Principles and Applications

The logging tools are described below. The acronyms and measurement units can be found in Table T3. Their principles, applications, and approximate vertical resolution are summarized in Table T4. More detailed information on individual tools and their geological applications may be found in Ellis (1987), Goldberg (1997), Lovell et al. (1998), Rider (1996), Schlumberger (1989, 1994), Serra (1984, 1986, 1989), and the LDEO-BRG Wireline Logging Services Guide (LDEO-BRG, 2000).

Natural Radioactivity

Two spectral gamma ray tools are usually used to measure and classify natural radioactivity in the formation—the NGT and the HNGS. The NGT uses a sodium iodide scintillation detector and five-window spectroscopy to determine concentrations of the three elements whose isotopes dominate the natural radiation spectrum—potassium (in weight percent), thorium (in parts per million), and uranium (in parts per million). High K and Th values indicate greater clay concentrations, and increased U values often indicate the presence of organic matter.

T3. Logging tool and measurement units and acronyms, p. 64.

T4. Logging tool specifications, p. 65.

The HNGS is similar to the NGT, but it uses two bismuth germanate scintillation detectors for a significantly improved tool precision.

The NGT response is sensitive to the borehole diameter. These diameter effects are corrected during postcruise processing.

Density

Formation density is determined from the density of electrons in the formation, which is measured with the HLDT. The tool contains a radioactive cesium (^{137}CS) gamma ray source (622 keV) and far and near gamma ray detectors mounted on a shielded skid, which is pressed against the borehole. Gamma rays emitted by the source undergo Compton scattering, which involves the transfer of energy from gamma rays to the electrons in the formation via elastic collisions. The number of scattered gamma rays that reach the detectors is directly related to the density of electrons in the formation, which is in turn related to bulk density. Porosity may also be derived from this bulk density if the matrix (grain) density is known.

The HLDT also measures the photoelectric effect factor (PEF) caused by absorption of low-energy gamma rays. Photoelectric absorption occurs when gamma rays reach <150 keV after being repeatedly scattered by electrons in the formation. Because PEF depends on the atomic number of the elements in the formation, it varies according to the chemical composition and is essentially independent of porosity. For example, the PEF of pure calcite = 5.08 b/e⁻; illite = 3.03 b/e⁻; quartz = 1.81 b/e⁻; and kaolinite = 1.49 b/e⁻. PEF values can be used in combination with NGT curves to identify different types of clay minerals. Coupling between the tool and borehole wall is essential for good HLDT logs. Poor contact results in underestimation of density values. Poor contact may occur when the borehole diameter is greater than the length of the caliper (e.g., for borehole diameters, >48 cm).

The depth of investigation into the formation of the lithodensity tool is of the order of tens of centimeters, depending on the density of the rock.

Porosity

Formation porosity, usually called neutron porosity, is measured with the APS. The sonde incorporates a minitron neutron generator that produces fast neutrons (14.4 MeV) and five neutron detectors (four epithermal and one thermal) positioned at differing intervals from the minitron. The measurement principle involves counting neutrons that arrive at the detectors after being slowed by neutron absorbers surrounding the tool. The highest energy loss occurs when neutrons collide with hydrogen nuclei, which have practically the same mass as the neutron (the neutrons simply bounce off heavier elements without losing much energy). If the hydrogen (i.e., water) concentration is small, as in low-porosity formations, neutrons can travel farther before being captured and the count rates increase at the detector. The opposite effect occurs when the water content is high. However, because hydrogen bound in minerals such as clays or in hydrocarbons also contributes to the measurement, the raw porosity value is often an overestimate.

Upon reaching thermal energies (0.025 eV), the neutrons are captured by the nuclei of Cl, Si, B, and other elements, resulting in a gamma ray emission. This neutron capture cross section (Σ_t) is also measured by the tool.

Electrical Resistivity

There exist two types of resistivity tool: the Dual Laterolog (DLL) and the DIT-E. The DLL, being a resistivity device, is most accurate in medium- to high-resistivity formations. The DIT-E, being a conductivity-sensitive device, is most accurate in low- to medium-resistivity formations. The DIT-E, however, is commonly used to measure the formation electrical resistivity.

The DIT-E has a deep-reading induction device (IDPH), a medium-reading induction device (IMPH), a spherically focused log device (SFLU), and an SP device. The two induction devices transmit high-frequency alternating currents through transmitter coils, creating time-varying magnetic fields that induce currents in the formation. These induced currents again create a magnetic field that induces new currents in the receiver coils, producing a voltage. These induced currents are proportional to the conductivity of the formation as is the voltage. The SFLU is a shallow-penetration galvanic device that measures the current necessary to maintain a constant voltage drop across a fixed interval of the formation. In high-resistivity formations ($>100 \Omega\text{m}$), both inductive IDPH and IMPH measurements may be erroneous, but the error can be greatly reduced by downhole calibration if a massive formation exists of exceedingly high resistivity. In such cases, SFLU measurements produce results of similar quality to the DLL device (Shipboard Scientific Party, 1998b). Grains and hydrocarbons are electrically resistive, whereas ionic solutions and clays are conductive.

Spontaneous potentials can originate from a variety of causes: electrochemical, electrothermal, and electrokinetic streaming potentials and membrane potentials because of differences in the mobility of ions in the pore and drilling fluids. SP may be useful to infer fluid flow zones and formation permeability.

Temperature, Acceleration, and Pressure

Downhole temperature, acceleration, and pressure are measured with the TAP tool. When attached to the bottom of the triple combo string, the TAP tool is run in an autonomous mode, with data stored in built-in memory. Two thermistors are mounted near the bottom of the tool to detect borehole fluid temperatures at different rates. A thin fast-response thermistor is able to detect small abrupt changes in temperature. A thicker slow-response thermistor is used to estimate temperature gradients and thermal regimes more accurately. The pressure transducer is included to activate the tool at a specified depth. A three-axis accelerometer measures tool movement downhole, providing data for analyzing the effects of heave on a deployed tool string, which should eventually lead to a finer adjustment of the WHC.

The borehole temperature record provides information on the thermal regime of the surrounding formation. The vertical heat flow can be estimated from the vertical temperature gradient combined with measurements of the thermal conductivity from core samples.

The temperature record must be interpreted with caution, as the amount of time elapsed between the end of drilling and the logging operation is generally not sufficient to allow the borehole to recover thermally from the influence of drilling fluid circulations. The data recorded under such circumstances may differ significantly from the thermal equilibrium of that environment. Nevertheless, from the spatial temperature gradient it is possible to identify abrupt temperature

changes that may represent localized fluid flow into the borehole, which is indicative of fluid pathways and fracturing and/or breaks in the temperature gradient that may correspond to contrasts in permeability at lithologic boundaries.

Acoustic Velocity

The DSI tool employs a combination of monopole and dipole transducers to make accurate measurements of sonic wave propagation in a wide variety of formations (Shipboard Scientific Party, 1998a). In addition to a robust and high-quality measurement of compressional wave velocity, the DSI excites a flexural mode in the borehole that can be used to estimate shear wave velocity even in highly unconsolidated formations. When the formation shear velocity is less than the borehole fluid velocity, particularly in unconsolidated sediments, the flexural wave travels at the shear wave velocity and is the most reliable way to estimate a shear velocity log. Meanwhile, the omnidirectional source generates compressional, shear, and Stoneley waves into hard formations. The configuration of the DSI also allows recording of both in-line and cross-line dipole waveforms. In many cases, the dipole sources could also result in estimates of shear wave velocity in hard rocks better than or equivalent to the monopole source. These combined modes can be used to estimate shear wave splitting caused by preferred mineral and/or structural orientation in consolidated formations. A low-frequency (80 Hz) source enables Stoneley waveforms to be acquired as well.

The DSI measures the transit times between sonic transmitters and an array of eight receiver groups with 15-cm spacing, each consisting of four orthogonal elements that are aligned with the dipole transmitters. During acquisition, the output from these 32 individual elements are differenced or summed appropriately to produce in-line and cross-line dipole signals or monopole-equivalent (compressional and Stoneley) waveforms, depending on the operation modes. The detailed description of tool configuration and data processing are described in the Leg 174B *Initial Reports* volume (Shipboard Scientific Party, 1998a).

Formation MicroScanner

The FMS provides high-resolution electrical resistivity-derived images of borehole walls. The tool has four orthogonal arms with pads, each containing 16 button electrodes that are pressed against the borehole wall during the recording. The electrodes are arranged in two diagonally offset rows of eight electrodes each and are spaced ~2.5 mm apart. A focused current is emitted from the four pads into the formation, with a return electrode near the top of the tool. Array buttons on each of the pads measure the current intensity variations. Processing transforms these measurements of the microresistivity variations of the formation into continuous, spatially oriented, and high-resolution images that mimic geologic structures behind the borehole walls. Further processing can provide measurements of dip and direction (azimuth) of planar features in the formation. FMS images are particularly useful for mapping structural features, dip determination, detailed core-log correlation, positioning of core sections with poor recovery, and analysis of depositional environments and stress distribution.

The FMS image is sensitive to structures as deep as ~25 cm beyond the borehole wall and has a maximum vertical resolution of 5 mm with

a coverage of 25% of the borehole wall for a borehole diameter of $9\frac{7}{8}$ in (i.e., RCB bit size). FMS logging commonly includes two passes, the images of which are merged to improve the borehole wall coverage. To produce reliable FMS images, however, the pads must be firmly pressed against the borehole wall. The maximum borehole deviation where good data can be recorded with this tool is 10° . Irregular borehole walls will also adversely affect the images because contact with the wall is poor.

Accelerometry and Magnetic Field Measurement

Three-component acceleration and magnetic field measurements are made with the GPIT. The primary purpose of this tool, which incorporates a three-component accelerometer and a three-component magnetometer, is to determine the acceleration and orientation of the FMS-sonic tool string during logging. The acceleration data allow more precise determination of log depths than is possible on the basis of cable length alone, as the wireline is subject to both stretching and ship heave. This provides a means of correcting the FMS images for irregular tool motion, allowing the true dip and direction (azimuth) of structures to be determined.

Vertical Seismic Profiles

Vertical seismic profile (VSP) experiments provide a crucial link in the increasing scale of observation (from core measurements to downhole logs to seismic reflection data) by tying the observed surface seismic reflectors to the subsurface layer interfaces. The VSP determines interval velocities at seismic frequencies, thereby bridging the gap between the sonic log and surface seismic data. In addition, seismic data are a function of time, whereas downhole logs are a function of depth; the VSP, which measures traveltime to known depths, establishes the time-depth relationship necessary to match the regional structural model inferred from seismic reflection data obtained from towed air guns and streamers. The first three-component borehole seismic experiment in the deep ocean was conducted during Deep Sea Drilling Project (DSDP) Leg 52 (Stephen et al., 1980). Three-component VSPs have also been conducted during ODP Legs 102, 109, 118, 123, 147, 148, and 165.

Zero-offset vertical seismic profiles were collected using the Schlumberger WST-3. The WST-3 is a modern seismic acquisition tool with three orthogonal geophones. The WST-3 has been successfully field tested in Texas. Leg 200 was the first ODP leg to use this tool. The available WST-3 tool specifications are given in Table T5. The WST is run separately from other logging runs because the tool is clamped at regular intervals in the borehole. It is run last because the clampings may damage the borehole wall. The seismic sources are triggered through the underway geophysics laboratory firing system described elsewhere.

After data acquisition, the data were recorded to tape and loaded in Schlumberger's GeoFrame software system for further processing.

T5. WST-3 tool specifications, p. 66.

Log Quality Control, Processing, and Analysis

Log Data Quality

The quality of several types of log data may be degraded by excessively wide sections of the borehole or by rapid changes in the hole diameter. If the borehole is irregular, wide, or there are many washouts, there may be problems with those tools that require good contact with the borehole wall (e.g., density, porosity, and FMS). In some cases, corrections can be applied to the original data to compensate for the effects of these conditions.

Log Depth Scales

The depth of the wireline logging measurements is determined from the length of the logging cable played out at the winch on the ship. The seafloor is identified on the natural gamma log by the abrupt reduction in gamma ray count at the water/sediment boundary (mudline). The coring depth (driller's depth) is determined from the known length of the BHA and pipe stands and the depth of the mudline, which is estimated from recovery, typically from the first or second core obtained at a site.

Discrepancies between the driller's depth and the wireline log depth occur because of core expansion, incomplete core recovery, inaccurate estimation of the mudline, drill pipe stretch in the case of drill pipe depth, cable stretch (~1 m/km), and cable slip in the case of log depth. Tidal changes in sea level, up to 1 m in the open ocean, will also have an effect. Precise core-log depth matching is difficult in zones where core recovery is low because of the inherent ambiguity of placing the recovered section within the cored interval.

Logs from different tool strings may also have depth mismatches, caused by either cable stretch or incomplete heave compensation during recording. Distinctive features recorded by the natural gamma tool, run on every tool string, provide relative depth offsets and thus a means of depth shifting for correlation between logging runs.

Data Processing

On completion of logging, data are loaded to the Schlumberger GeoQuest's GeoFrame software system in the DHML for onboard preliminary interpretation. Basic processing is completed postcruise to provide a quality-controlled downhole logging data set that can be used for comparison, integration, and correlation with other data collected during each ODP leg. The processing includes depth adjustments to remove depth offsets between data from different logging runs, corrections specific to certain tools and logs, documentation for the logs (with an assessment of log quality), and conversion of the data to a widely accessible format (ASCII for the conventional logs and GIF for the FMS images). The GeoFrame software package is used for most of the processing.

ASCII versions of processed acoustic, caliper, density, gamma ray, magnetic, neutron porosity, resistivity, and temperature data are available (see the "[Related Leg Data](#)" contents list).

Core-Log-Seismic Integration

GeoFrame's IESX seismic interpretation software package is used to display site-survey seismic sections acquired precruise. Velocity and density logs collected during Leg 200 are used to create synthetic seismograms, which are compared with the seismic section and used to refine the depth-traveltime relation. In this way, seismic reflectors and sequences are correlated with log units and the lithostratigraphic units in the core. Further detailed processing, analysis, and interpretation are completed postcruise.

UNDERWAY GEOPHYSICS

While transiting from Site 1223 to Site 1224 and from Site 1224 to San Diego, we conducted 3.5-kHz echo sounding and magnetometer surveys. In addition, as we approached and departed Site 1224, we shot single-channel seismic reflection lines within 66 km of the site.

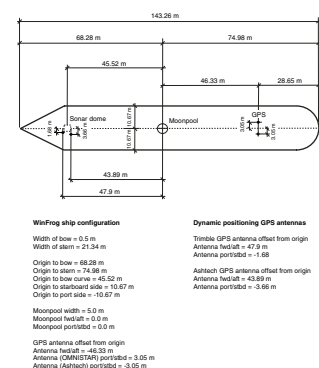
Navigation data were acquired throughout the leg on an Ashtech GG24 Global Positioning System (GPS) receiver. The antenna was mounted on the starboard stack 46.33 m aft of the moonpool (Fig. F15). The datum is the moonpool. GPS fixes were recorded by WinFrog navigation software every 60 s except during water gun shooting, when they were recorded at each shot instant. Generic Mapping Tools (GMT) software (Wessel and Smith, 1995) on Sun Sparc 10 UNIX workstations was used to process and display the navigation data.

The time datum for all underway geophysics activities is Universal Time Coordinated (UTC) (similar to Greenwich mean time) as provided from the Ashtech receivers. If communication between the Ashtech receiver and the satellite is interrupted, the receiver uses its own internal clock to maintain the time base. The WinFrog navigation system displays the UTC time many times per second, but the internal clock is not being synchronized to UTC. During this cruise we used the WinFrog navigation system to send a trigger pulse to the water gun based on WinFrog's internal clock. The blast phone pulse is then used to start the acquisition in the A2D software from the University of Hawaii. The time stamp on the seismic data comes from the Sun internal clock, which is manually synchronized with UTC. So data acquired in A2D have time referenced approximately to UTC. The trigger pulses from WinFrog, however, are based on the WinFrog clock, which may not be precisely UTC. Time constraints did not permit calibrating the various time bases against UTC during the cruise.

The magnetic data were acquired with an EG&G Geometrics Marine Proton Magnetometer (model G-886) towed 500 m behind the ship. Values of total field intensity were acquired every 60 s using the WinFrog navigation software on a Windows PC.

The underway 3.5-kHz echo sounder data were acquired using the hull-mounted EDO transceiver with a multielement 10-kW transducer as both the source and receiver. The 3.5-kHz transducer consists of six elements mounted on the ship's hull 45.5 m forward of the moonpool and is described in more detail in "Onsite Geophysics," p. 35. The data were processed in real time using a Raytheon CESP III (Correlator Echo Sounder Processor). The underway echo sounder data were not digitized but were recorded on an EPC 9802 analog line scan thermal paper recorder. The ship's speed, heading, and position were annotated on the EPC recorders and were logged each minute on WinFrog. The paper re-

F15. Summary of the significant dimensions necessary to correct the GPS location of various antennas to the moonpool, p. 58.



corder was gated to a depth range of 4500–5250 uncorrected meters, and uncorrected depths were logged at 5-min intervals by hand.

Uncorrected depths convert traveltime to nominal depth assuming a velocity of 1500 m/s. Corrected depths (using Matthews' Tables to allow for the varying sound speed with depth and location in the ocean [Carter, 1980]) were computed by hand for each site. For example, an uncorrected depth of 4967 m at the H2O site (area 51 in Matthews' Tables) corresponds to a corrected depth of 4979 m. An uncorrected depth of 4250 m at the Nuuanu site (area 52 in Matthews' Tables) corresponds to a corrected depth of 4250 m (i.e., no change).

The transducer elements are 0.9 m below the keel of the ship and 18.4 m below the dual elevator stool (the reference datum for drilling activities). Water depth relative to sea level was obtained by adding 0.9 m and the mean draft (typically 6.5 ± 0.6 m) to the corrected echo sounder depth. Figure F16 is a schematic of the ship that summarizes some of the key dimensions used in computing depth to various datums. The shipboard 12-kHz system had poor signal-to-noise characteristics and was not used during this leg.

A program called "U/W Watch" was developed by ODP to configure the acquisition sequences for the echo sounder and the magnetometer and to display and annotate the echo sounder output on the EPC graphic recorders. This program is written in the National Instruments LabView language and runs on a Compaq Deskpro Workstation.

A Seismic Systems Inc. "T Water Gun" (Type S80 model 1; 80 in³) was fired at 10-s intervals as a source for the single-channel seismic reflection studies as well as for shallow refraction surveys to the H2O broadband seafloor seismometer. Water gun depth was estimated at 4 m (Fig. F17). Shot instants and navigation were acquired on the WinFrog navigation system.

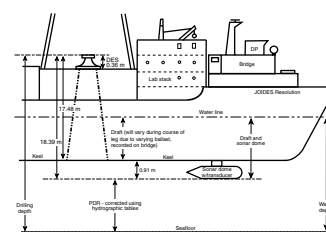
Data from the H2O seismometer (Chave et al., 1997; Duennebie et al., 2000) were continuously acquired in real time at the University of Hawaii, and files were downloaded to the ship daily. The data can be analyzed in a similar fashion to data from radio sonobuoys (Knott and Hoskins, 1975).

The single-channel streamer used was a Teledyne Exploration model 178 hydrophone string; it consisted of 60 elements at a spacing of 1.45 m and was towed 225 m (to the midpoint) behind the ship (Fig. F17). Streamer depth was estimated as 15 m. Data were acquired to 4-mm DAT tape and 8-mm Exabyte tape in SEG-Y format and were displayed in real time using the SIOSEIS software package (Henkart, 1992) running on a Sun UNIX work station. The hydrophone streamer malfunctioned during the approach survey because of a corroded connector.

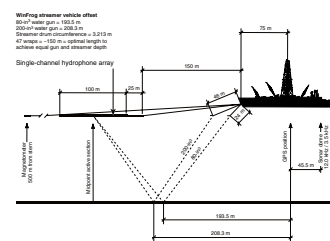
ONSITE GEOPHYSICS

Two styles of onsite 3.5-kHz experiments were conducted. In the first, we simply ran the 3.5-kHz echo sounder while the ship was effectively stationary. In the second, we lowered a 3.5-kHz (actually 4.252-kHz) pinger on the vibration-isolated television (VIT) frame. In this configuration, the pinger source was near the seafloor and the direct water wave and seafloor reflections were received on the ship's 3.5-kHz hull-mounted transducer.

F16. Significant depth dimensions on the ship, p. 59.



F17. Significant depths and ranges for the single-channel seismic acquisition system and magnetometer system, p. 60.



Onsite Conventional 3.5-kHz Echo Sounding

The recording was made using a Raytheon model PTR105B 2-kW transceiver with a CESP-III. The outgoing signal was a 100-ms chirp. The ship's 3.5-kHz transducer consists of a 16-in ring of piezoelectric elements and is located in a sonar pod that extends ~1 m below the midline of the hull at frame 43. Its half-power beamwidth is ~35°, far greater than the pitch or roll of the ship. The recordings were made on an EPC Labs 20-in graphic recorder (model 9802).

Deep-Source Experiment

Determining the thickness and attitude of the seafloor sediments acoustically before spudding-in can facilitate the determination of suitable drilling sites. For example, a minimum sediment cover of 10 m is needed to set a reentry cone and casing. Reflections from sediment interfaces beneath the seafloor are commonly observed on ship's echo sounder recordings using transducers in the range of 1 to 5 kHz. These returns can come from a variable area depending on the depth and roughness of the seafloor and the acoustic interfaces beneath it. For this reason, in deep water the lateral extent of the subseafloor reflections observed can be difficult to determine from soundings made from a ship. To reduce the area insonified, the sounding transducer can be lowered near the seafloor, thereby permitting a better determination of the sediment thickness and the lateral extent of seafloor reflectors at a specific drill site.

The VIT frame is used to visually survey the seafloor in preparation for spudding-in and reentering holes fitted with a reentry cone. It provides an ideal vehicle with which to make "close-up" acoustic surveys of drill sites. An ORE Accusonic pinger (model 263), consisting of a 4.252-kHz transducer interconnected with a 5-in-diameter, 33-in-long pressure housing containing a battery pack, a storage capacitor, and electronics, was mounted on the VIT frame (Fig. F18). This free-running pinger produces a 2-ms pulse at a 1-s repetition rate. Its half-power beam width is 65°. To distinguish it from other sonic devices, each ninth ping is skipped. The transducer's active face is about one-third of the wavelength of its characteristic frequency; therefore, there is only a single front and rear lobe to its directivity pattern.

The shipboard recording was made on the EPC model 9802 graphic recorder running at a 1-s sweep, the same periodicity as the pinger. The recordings were ungated. The ship's outgoing signal was turned off. Because the 1-s repetition rate is less than the reflection traveltime to the seafloor, there are multiple concurrent reflection sequences in the water column. For seafloor depths between 4500 and 5250 m, there are seven reflection sequences. The trace offset in the skipped ping recording sweeps allows determining which 750-m depth interval the pinger is in during the lowering.

The pinger was lowered six times on the VIT frame to 4935 m water depth at Site 1224. The direct and reflected returns were received on the *JOIDES Resolution's* 3.5-kHz transducers. The direct water wave arrival from the back (upward facing) lobe of the transducer to the ship's transducers was readily visible on the recordings throughout the lowering. The reflection from the seafloor from the main (downward facing) lobe of the transducer was faintly visible when the VIT frame was near the surface, and it became progressively stronger as the frame was lowered. With the VIT frame near the seafloor, coherent returns were observed at

F18. The 4.252-kHz transducer, pinger batteries, and electronics on the VIT frame, p. 61.



traveltimes as great as 40 ms beneath the seafloor. The reflections from the reentry cone and casing landing tool could readily be seen during the course of jetting in the cone and 20-in diameter casing string in Hole 1224D. In a subsequent lowering to set 10³/₄-in casing, the casing landing tool could also be seen.

Thruster 3 of the ship's 12 athwartship thrusters is located on the port side of the ship at frame 43. At times, the wash from this thruster across the 3.5-kHz transducer degraded the acoustic reception.

We suggest that this sonic observational tool could be useful in optimally locating future reentry sites where there is modest sediment cover.

REFERENCES

- Balsam, W.L., and Damuth, J.E., 2000. Further investigations of shipboard vs. shore-based spectral data: implications for interpreting Leg 164 sediment composition. *In* Paull, C.K., Matsumoto, R., Wallace, P., and Dillon, W.P. (Eds.), *Proc. ODP, Sci. Results*, 164: College Station, TX (Ocean Drilling Program), 313–324.
- Balsam, W.L., Damuth, J.E., and Schneider, R.R., 1997. Comparison of shipboard vs. shore-based spectral data from Amazon-Fan cores: implications for interpreting sediment composition. *In* Flood, R.D., Piper, D.J.W., Klaus, A., and Peterson, L.C. (Eds.), *Proc. ODP, Sci. Results*, 155: College Station, TX (Ocean Drilling Program), 193–215.
- Balsam, W.L., Deaton, B.C., and Damuth, J.E., 1998. The effects of water content on diffuse reflectance measurements of deep-sea core samples: an example from ODP Leg 164 sediments. *Mar. Geol.*, 149:177–189.
- Blum, P., 1997. Physical properties handbook: a guide to the shipboard measurement of physical properties of deep-sea cores. *ODP Tech. Note*, 26 [Online]. Available from World Wide Web: <<http://www-odp.tamu.edu/publications/tnotes/tn26/INDEX.HTM>>. [Cited 2001-12-11]
- Boggs, S., 1995. *Principles of Sedimentology and Stratigraphy* (2nd ed.): Upper Saddle River, NJ (Prentice-Hall, Inc.).
- Boyce, R.E., 1976. Definitions and laboratory techniques of compressional sound velocity parameters and wet-water content, wet-bulk density, and porosity parameters by gravimetric and gamma-ray attenuation techniques. *In* Schlanger, S.O., Jackson, E.D., et al., *Init. Repts. DSDP*, 33: Washington (U.S. Govt. Printing Office), 931–958.
- Cande, S.C., and Kent, D.V., 1995. Revised calibration of the geomagnetic polarity timescale for the Late Cretaceous and Cenozoic. *J. Geophys. Res.*, 100:6093–6095.
- Carter, D.J.T., 1980. Echo-sounding correction tables (formerly Matthews' Tables): Taunton, Somerset, UK (Hydrographic Dept., Min. of Defence).
- Chave, A.D., Butler, R., Petitt, R.A., Jr., Yoerger, D.R., Wooding, F.B., Bowen, A.D., Freitag, L.E., Catipovic, J., Duennebier, F.K., Harris, D., Dodeman, A.H., and Brewer, S.T., 1997. H2O: the Hawaii-2 Observatory. *Proceedings of the International Workshop on the Scientific Use of Submarine Cables*: Okinawa (Japan Print Center), 114–118.
- Duennebier, F.K., Butler, R., Chave, A., Harris, D., Jolly, J., and Babinec, J., 2000. Broadband seismograms from the Hawaii-2 Observatory [paper presented at Am. Geophys. Union Mtg., San Francisco, Fall 2000].
- Ellis, D.V., 1987. *Well Logging for Earth Scientists*: New York (Elsevier).
- Goldberg, D., 1990. Test performance of the Ocean Drilling Program wireline heave motion compensator. *Sci. Drill.*, 1:206–209.
- , 1997. The role of downhole measurements in marine geology and geophysics. *Rev. Geophys.*, 35:315–342.
- Henkart, P., 1992. SIOSEIS—a computer system for enhancing and manipulating marine seismic reflection and refraction data. *Scripps Inst. of Oceanogr.* [Online]. Available from World Wide Web: <<http://sioseis.ucsd.edu>>.
- Hoppie, B.W., Blum, P., and the Shipboard Scientific Party, 1994. Natural gamma-ray measurements on ODP cores: introduction to procedures with examples from Leg 150. *In* Mountain, G.S., Miller, K.G., Blum, P., et al., *Proc. ODP, Init. Repts.*, 150: College Station, TX (Ocean Drilling Program), 51–59.
- Knott, S.T., and Hoskins, H., 1975. Collection and analysis of seismic wide angle reflection and refraction data using radio sonobuoys. *Woods Hole Oceanographic Institution Technical Memorandum*, WHOI-75-33.
- Lamont-Doherty Earth Observatory Borehole Research Group, 2000. *ODP Logging Manual: An Electronic Guide to ODP Logging Services*, v 2.0, [CD-ROM]. Available from: Lamont-Doherty Earth Observatory, Columbia University, Palisades NY 10964, USA.

- Lovell, M.A., Harvey, P.K., Brewer, T.S., Williams, C., Jackson, P.D., and Williamson, G., 1998. Application of FMS images in the Ocean Drilling Program: an overview. *In* Cramp, A., MacLeod, C.J., Lee, S.V., and Jones, E.J.W. (Eds.), *Geological Evolution of Ocean Basins: Results from the Ocean Drilling Program*. Spec. Publ.—Geol. Soc. London, 131:287–303.
- MacKenzie, W.S., Donaldson, C.H., and Guilford, C., 1982. *Atlas of Igneous Rocks and Their Textures*: Harlow, England (Longman).
- Mazzullo, J., and Graham, A.G. (Eds.), 1988. Handbook for shipboard sedimentologists. *ODP Tech. Note*, 8.
- Mazzullo, J.M., Meyer, A., and Kidd, R.B., 1988. New sediment classification scheme for the Ocean Drilling Program. *In* Mazzullo, J., and Graham, A.G. (Eds.), *Handbook for Shipboard Sedimentologists*. ODP Tech. Note, 8:45–67.
- Munsell Color Company, Inc., 1994. *Munsell Soil Color Chart* (Revised ed.): Newburgh, MD (Munsell Color).
- Murray, R.W., Miller, D.J., and Kryc, K.A., 2000. Analysis of major and trace elements in rocks, sediments, and interstitial waters by inductively coupled plasma–atomic emission spectrometry (ICP-AES). *ODP Tech. Note*, 29 [Online]. Available from World Wide Web: <<http://www-odp.tamu.edu/publications/tnotes/tn29/INDEX.HTM>>. [Cited 2001-12-11]
- Rider, M., 1996. *The Geological Interpretation of Well Logs* (2nd ed.): Caithness (Whittles Publishing).
- Rothwell, R.G., 1989. *Minerals and Mineraloids in Marine Sediments: An Optical Identification Guide*: Basking, UK (Elsevier Appl. Sci. Publ.).
- Schlumberger, 1989. *Log Interpretation Principles/Applications*: Houston (Schlumberger Educ. Services), SMP-7017.
- , 1994. *IPL Integrated Porosity Lithology*: Houston (Schlumberger Wireline and Testing), SMP-9270.
- Schlumberger, C., Schlumberger, E.H.M., and Leonardon, E.G., 1934. Electric coring: a method of determining bottom-hole data by electrical measurement. *Trans. AIME*, 110:237–272.
- Serra, O., 1984. *Fundamentals of Well-Log Interpretation* (Vol. 1): *The Acquisition of Logging Data*: Dev. Pet. Sci., 15A.
- , 1986. *Fundamentals of Well-Log Interpretation* (Vol. 2): *The Interpretation of Logging Data*. Dev. Pet. Sci., 15B.
- , 1989. *Formation MicroScanner Image Interpretation*: Houston (Schlumberger Educ. Services), SMP-7028.
- Shipboard Scientific Party, 1998a. Introduction. *In* Becker, K., Malone, M.J., et al., *Proc. ODP, Init. Repts.*, 174B: College Station, TX (Ocean Drilling Program), 3–9.
- , 1998b. Site 395. *In* Becker, K., Malone, M.J., et al., *Proc. ODP, Init. Repts.*, 174B: College Station, TX (Ocean Drilling Program), 13–23.
- , 2000a. Explanatory notes. *In* Coffin, M.F., Frey, F.A., Wallace, P.J., et al., *Proc. ODP, Init. Repts.*, 183, 1–94 [CD-ROM]. Available from: Ocean Drilling Program, Texas A&M University, College Station, TX 77845-9547, U.S.A.
- , 2000b. Explanatory notes. *In* Sacks, I.S., Suyehiro, K., Acton, G.D., et al., *Proc. ODP, Init. Repts.*, 186, 1-51 [CD-ROM]. Available from: Ocean Drilling Program, Texas A&M University, College Station TX 77845-9547, USA.
- , 2001. Explanatory notes. *In* Christie, D.M., Pedersen, R.B., Miller, D.J., et al., *Proc. ODP, Init. Repts.*, 187, 1–42 [CD-ROM]. Available from: Ocean Drilling Program, Texas A&M University, College Station TX 77845-9547, USA.
- , 2002. Explanatory notes. *In* Tarduno, J.A., Duncan, R.A., Scholl, D.W., et al., *Proc. ODP, Init. Repts.*, 197, 1–89 [CD-ROM]. Available from: Ocean Drilling Program, Texas A&M University, College Station TX 77845-9547, USA.
- Stephen, R.A., Loudon, K.E., and Matthews, D.H., 1980. The oblique seismic experiment on DSDP Leg 52. *Geophys. J. R. Astron. Soc.*, 60:289–300.

- Terry, R.D., and Chilingar, G.V., 1955. Summary of "Concerning some additional aids in studying sedimentary formations" by M.S. Shvetsov. *J. Sediment. Petrol.*, 25:229–234.
- Vacquier, V., 1985. The measurement of thermal conductivity of solids with a transient linear heat source on the plane surface of a poorly conducting body. *Earth Planet. Sci. Lett.*, 74:275–279.
- Von Herzen, R.P., and Maxwell, A.E., 1959. The measurement of thermal conductivity of deep-sea sediments by a needle-probe method. *J. Geophys. Res.*, 64:1557–1563.
- Wentworth, C.K., 1922. A scale of grade and class terms of clastic sediments. *J. Geol.*, 30:377–392.
- Wessel, P., and Smith, W.H.F., 1995. New version of the Generic Mapping Tools released. *Eos, Trans. Am. Geophys. Union*, 76:329.

Figure F1. Schematic illustrating hole, core, and section labeling.

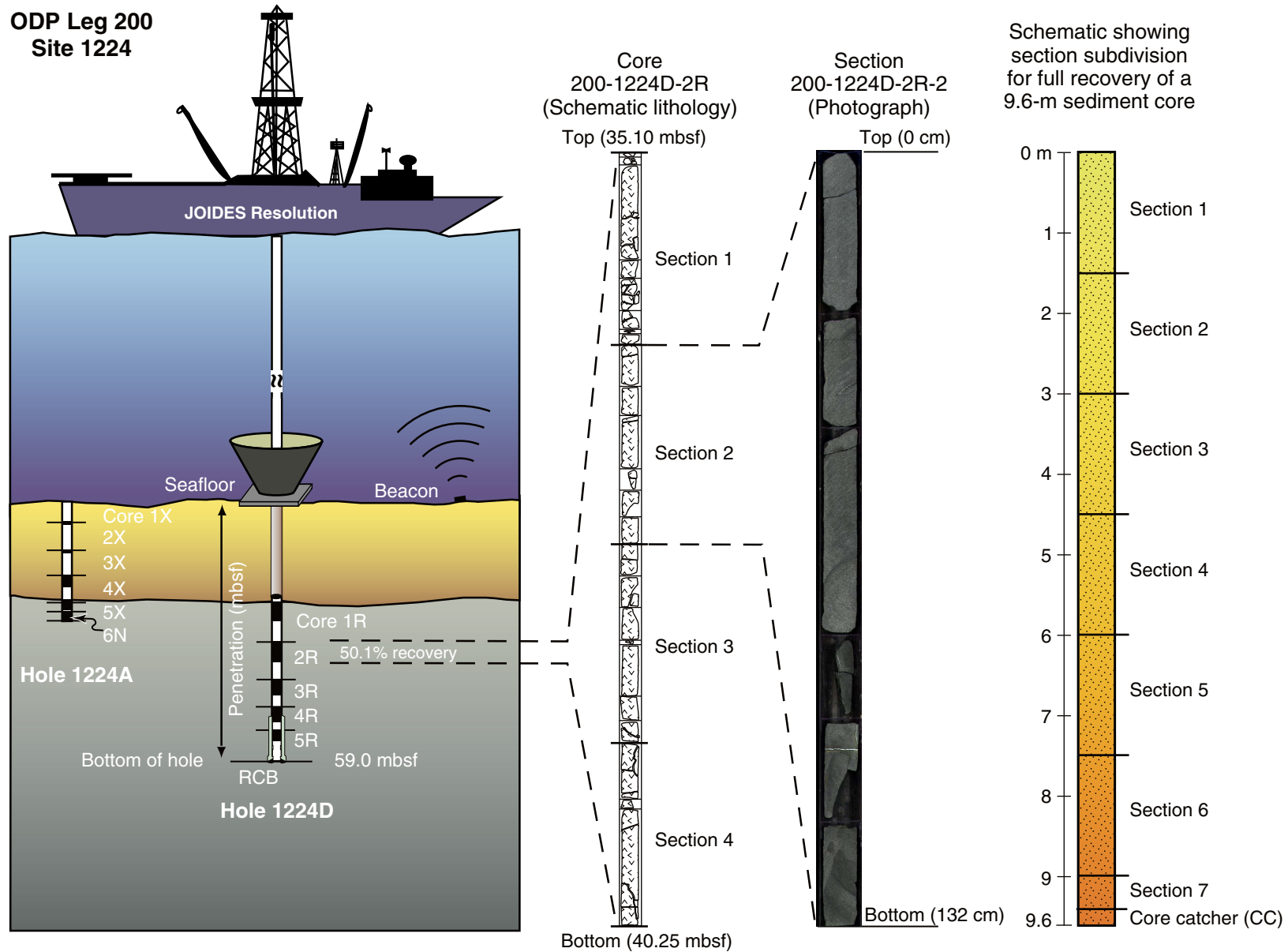


Figure F2. Example of an electronic visual core description form (eVCD) used for sediments (AppleCORE sheet).

| Site 1223 Hole A Core 1H Cored 0.0-7.7 mbsf | | | | | | | | | | | |
|---|---------|---------------|----------|-----------|-------------|--------|---------|----------|--------|-----------|---|
| METERS | SECTION | GRAPHIC LITH. | BIOTURB. | STRUCTURE | ACCESSORIES | ICHNO. | FOSSILS | DISTURB. | SAMPLE | COLOR | DESCRIPTION |
| 1 | 1 | | | | | | | | SS | dk ye BR | DARK YELLOWISH BROWN CLAY and DARK VOLCANICLASTIC TURBIDITES |
| 1 | | | | | | | | | SS | .. | |
| 2 | 2 | | | | | | | | SS | dk BR | Section 1, 86-101 cm: Black volcaniclastic turbidites (10YR 2/1) with fine sand normally graded to silt, bioturbated at the top and with a sharp erosional basal contact. |
| 2 | | | | | | | | | SS | .. | |
| 3 | 3 | | | | | | | | SS | vdk gy BR | Section 2, 61-103 cm: Volcaniclastic turbidite, black at the base (10YR 2/1 at 100 cm) and very dark grayish brown near the top (10YR 3/2), sandy silt to fine grained sand, mineral clasts and glass fragments presents. |
| 3 | | | | | | | | | SS | BK | |
| 4 | 3 | | | | | | | | SS | .. | |
| 4 | | | | | | | | | SS | BR | Section 2, 148-150 cm: Volcaniclastic turbidite. |
| 5 | 4 | | | | | | | | SS | BR | Section 3, 76-99 cm: Very dark grayish brown (10YR 3/2) turbidite with a sharp basal contact, fining upward, and composed of very fine sand with some oxide staining. |
| 6 | 4 | | | | | | | | SS | vdk gy BR | Section 4, 40-67 cm: Transition zone from clay to turbidite with color banding; darker bands are coarser silty clay and lighter bands are clay. |
| 7 | 5 | | | | | | | | SS | gy BK BR | Section 4, 67 cm to Section 5, 78 cm: Turbidites; silty sand and very fine sand. |
| 7 | | | | | | | | | SS | .. | |
| | | | | | | | | | SS | .. | |
| | | | | | | | | | SS | vdk gy BR | Section 5, 114-121 cm: Granular sand; very disturbed and may only be 3 cm thick (117-120 cm) (thin section sample). Radiolarians present. |
| | | | | | | | | | | | Section 5, 131 cm to base of section: very dark brown clay mixed with sand, highly disturbed by drilling. |
| | | | | | | | | | | | Section CC: Sandy clay underlain by dark brown to dark reddish brown clay. |

Figure F3. Key to electronic volcanoclastic visual core description form (eV-VCD).

Volcanoclastic texture/structure definitions and abbreviations

Grain size:

- cl = clay
- s cl = silty clay
- cl s = clayey silt
- s = silt
- sa s = sandy silt
- m = medium sand
- c = coarse sand
- vc = very coarse sand
- m-c = medium to coarse sand
- c-vc = coarse to very coarse sand
- g = granule
- p = pebble

Size grading:

- Normal = fining upward
- Reverse = fining downward
- Massive = massively bedded, or not graded

Disturbance:

- S = slight
- M = moderate
- H = high

Groundmass/grain size:

- g = glass
- vfg = very fine grained (<0.5 mm)
- fg = fine grained (0.5-1 mm)
- mg = medium grained (1-2 mm)

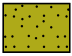

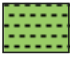


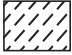
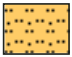

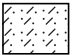
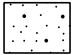
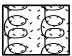
Shipboard studies:

- TSB = thin section billet
- ICP = inductively coupled plasma
- PP = physical properties
- XRD = X-ray diffraction
- Pmag = paleomagnetism
- WRB = whole-round microbiology
- SS = smear slide

Contact/boundary:

- S = sharp
- G = gradual

Rock classifications:

- | | | | |
|---|-------------------------------|---|---------------------|
|  | Silty claystone |  | Volcanoclastic silt |
|  | Clay |  | Silty sand |
|  | Silty clay |  | Basalt |
|  | Sandy silt |  | Clayey siltstone |
|  | Sandy clay |  | Sandy siltstone |
|  | Disturbed altered vitric tuff | | |

Depositional structures:



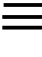



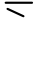



- | | | | |
|---|-----------------------|---|------------------------|
|  | Cross bedding |  | Normal-graded bedding |
|  | Planar laminations |  | Reverse-graded bedding |
|  | Vugs |  | Radiolarians |
|  | Veins |  | Spicules |
|  | Bioturbation | | |
|  | Disturbed by drilling | | |

Figure F4. Example of an electronic volcanoclastic rock visual core description form (eV-VCD).

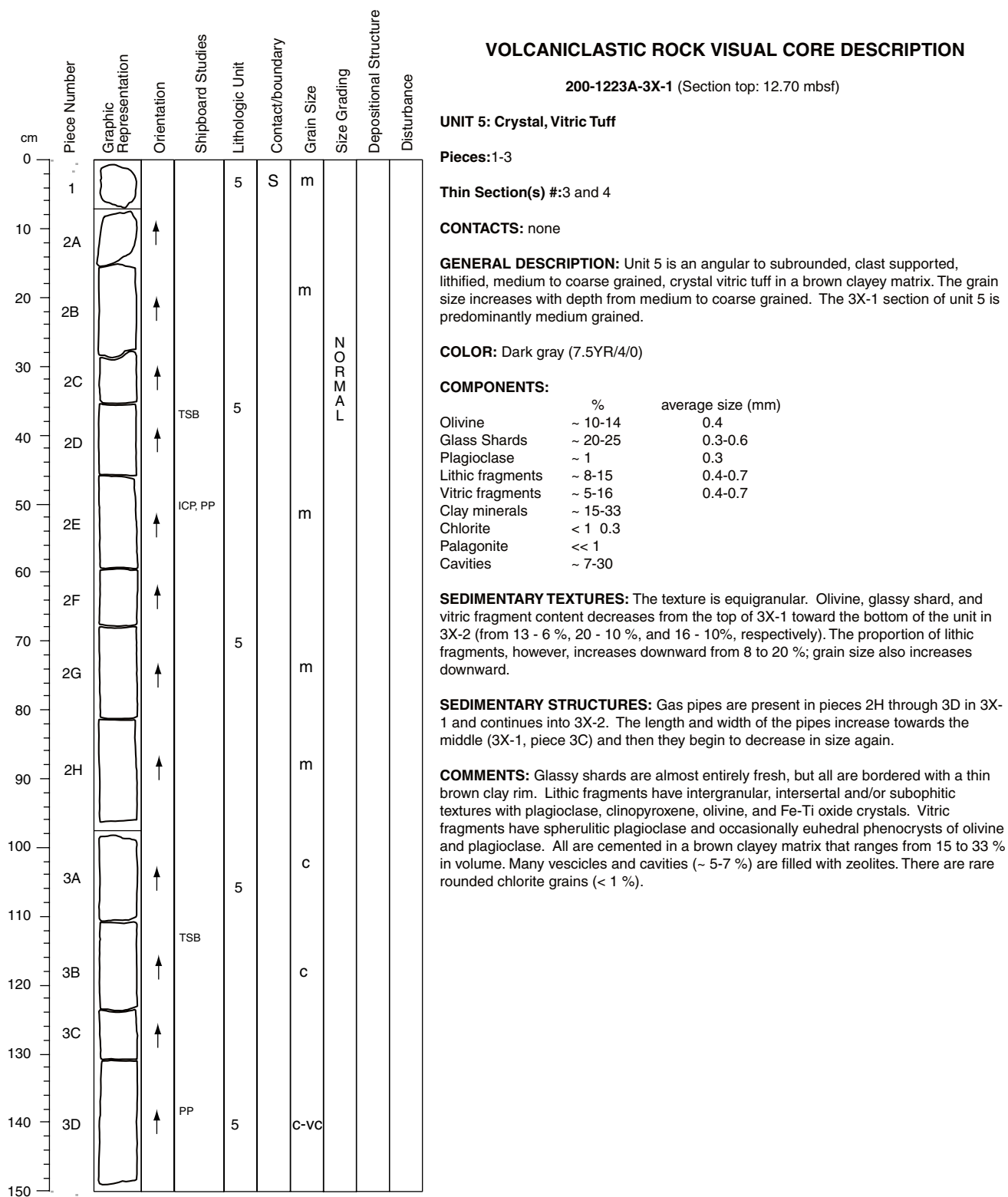


Figure F5. Key to electronic hard rock visual core description form (eHR-VCD).

Igneous texture/structure definitions and abbreviations





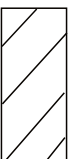


| | | | | | | |
|---------------------------|---|---------------------------------|---|--|---|--------------------|
| Phenocryst |  | a Aphyric (<1%) | sp Sparsely phyric (1%-2%) | mp Moderately phyric (3%-10%) | hp Highly phyric (>10%) | |
| Groundmass/ grain size |  | g Glass | vfg Very fine grained (<0.5 mm) | fg Fine grained (0.5-1 mm) | mg Medium grained (1-2 mm) | |
| Vesicularity |  | nv Non vesicular (<1%) | spv Sparsely vesicular (1%-5%) | mov Moderately vesicular (6%-20%) | hiv Highly vesicular (>20%) | |
| Vesicle structure |  | ev Empty vesicles | fv Filled vesicles | efv Empty and filled vesicles | | |
| Degree of alteration |  | Slight (2%-10%) |  | Moderate (>10%-40%) |  | High (>40%-80%) |

Figure F6. Example of an electronic hard rock visual core description form (eHR-VCD).

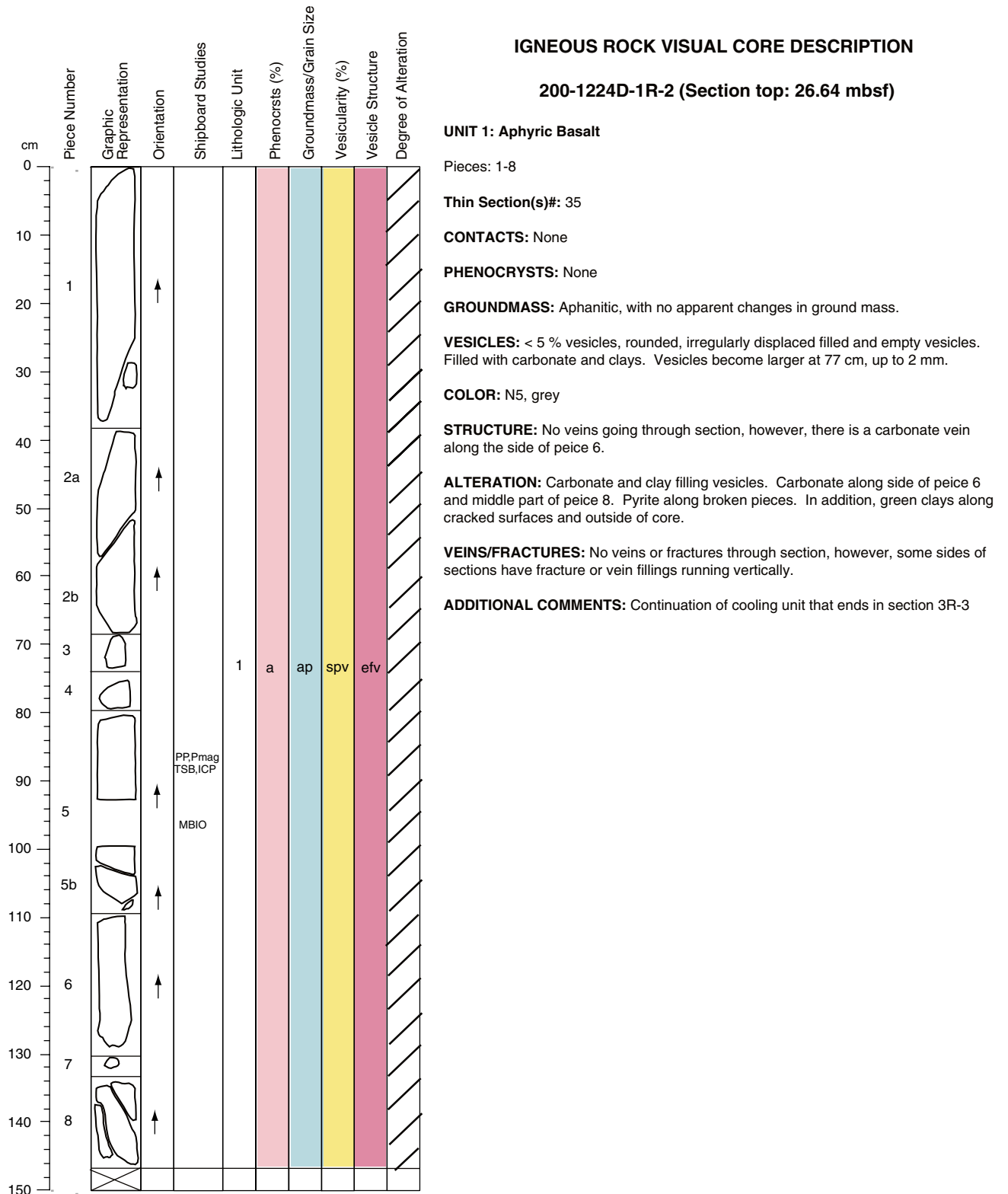


Figure F7. Udden-Wentworth grain-size classification scheme (Wentworth, 1922).

| Millimeters (mm) | Micrometers (μm) | Phi (ϕ) | Wentworth size class | Rock type |
|------------------|-------------------------------|----------------|----------------------|--------------------------|
| 4096 | | -12.0 | Boulder | Conglomerate/ Breccia |
| 256 | | -8.0 | Cobble | |
| 64 | | -6.0 | Pebble | |
| 4 | | -2.0 | Granule | |
| 2.00 | | -1.0 | | |
| 1.00 | | 0.0 | Very coarse sand | Sandstone |
| 0.50 | 500 | 1.0 | Coarse sand | |
| 0.25 | 250 | 2.0 | Medium sand | |
| 0.125 | 125 | 3.0 | Fine sand | |
| 0.0625 | 63 | 4.0 | Very fine sand | |
| 0.031 | 31 | 5.0 | Coarse silt | Siltstone |
| 0.0156 | 15.6 | 6.0 | Medium silt | |
| 0.0078 | 7.8 | 7.0 | Fine silt | |
| 0.0039 | 3.9 | 8.0 | Very fine silt | |
| 0.0006 | 0.06 | 14.0 | Clay | Claystone |





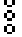
Figure F8. AppleCORE key used for sediments (eVCD).

Sedimentary texture/structure definitions and abbreviations

Color abbreviations:

dk = Dark
vdk = Very dark
ye = Yellowish
gy = Grayish
BR = Brown
BK = Black

Symbols:

 Graded bed (fining upward)
 Sponge spicules
 Radiolarian
 Disturbed by drilling
 Soupy

Samples:

SS = Smear slide
TS = Thin section
XRD = X-ray diffraction
MBIO = Microbiology
ICP = Inductively coupled plasma

Classifications:



Clay



Volcaniclastic silt



Sandy silt



Volcaniclastic sand



Sand-silt-clay



Sand

Figure F9. Example of a smear slide description form.

Smear Slide Descriptions

| Sample | | | | | | | Lithology | Texture | | | Mineral | | | Biogenic | | Comments |
|--------|---|-----|----|-----|-------|-------|-----------|---------|------|------|---------------|-------------------|----------------------------|---------------------|--|----------|
| Site | H | Cor | CT | Sct | Top | Depth | | Sand | Silt | Clay | Olivine (136) | Plagioclase (159) | Volcanic Glass Shard (247) | Radio-larians (173) | Siliceous Sponge Spicules (185) | |
| 1223 | A | 1 | H | 1 | 42.0 | 0.42 | D | | 10 | 90 | 5 | 10 | | | mostly clay minerals | |
| 1223 | A | 1 | H | 1 | 95.0 | 0.95 | D | 90 | 10 | | 40 | 50 | 10 | | | |
| 1223 | A | 1 | H | 1 | 125.0 | 1.25 | D | 20 | | 80 | 10 | 5 | 10 | | | |
| 1223 | A | 1 | H | 2 | 3.0 | 1.53 | D | 30 | 10 | 60 | 5 | 5 | 10 | | | |
| 1223 | A | 1 | H | 2 | 31.0 | 1.81 | D | 40 | | 60 | 5 | 5 | 10 | | aggregations of clay minerals | |
| 1223 | A | 1 | H | 2 | 57.0 | 2.07 | D | 20 | | 80 | 10 | | | 25 | | |
| 1223 | A | 1 | H | 2 | 58.0 | 2.08 | D | 90 | 10 | | 50 | 5 | 10 | 1 | | |
| 1223 | A | 1 | H | 2 | 65.0 | 2.15 | D | 90 | 10 | | 40 | 5 | 40 | | | |
| 1223 | A | 1 | H | 2 | 100.0 | 2.50 | D | 90 | 10 | | 40 | | 40 | | | |
| 1223 | A | 1 | H | 2 | 105.0 | 2.55 | D | 70 | 30 | | 5 | | 1 | 10 | spicule fragment very small | |
| 1223 | A | 1 | H | 2 | 146.0 | 2.96 | D | 75 | 25 | | 10 | 5 | 5 | 1 | 1 | |
| 1223 | A | 1 | H | 2 | 149.0 | 2.99 | D | 40 | 60 | | 60 | | 40 | 1 | 1 | |
| 1223 | A | 1 | H | 3 | 13.0 | 3.13 | D | | 30 | 70 | 10 | | 5 | | | |
| 1223 | A | 1 | H | 3 | 97.0 | 3.97 | D | 100 | | | 60 | | 40 | | grains mostly angular | |
| 1223 | A | 1 | H | 3 | 100.0 | 4.00 | D | | | 100 | 5 | | 1 | | spicules rare | |
| 1223 | A | 1 | H | 4 | 22.0 | 4.72 | D | | | 100 | 1 | | | | | |
| 1223 | A | 1 | H | 4 | 100.0 | 5.50 | D | 100 | | | 40 | 20 | 40 | 1 | | |
| 1223 | A | 1 | H | 5 | 10.0 | 6.10 | D | 30 | | 70 | 20 | 15 | 10 | | | |
| 1223 | A | 1 | H | 5 | 17.0 | 6.17 | D | 65 | 35 | | 40 | | 30 | 10 | 1 | |
| 1223 | A | 1 | H | 5 | 61.0 | 6.61 | D | 90 | 10 | | 40 | | 60 | | 1 | |
| 1223 | A | 1 | H | 5 | 74.0 | 6.74 | D | 80 | 20 | | 40 | | 60 | 5 | 1 | |
| 1223 | A | 1 | H | 5 | 87.0 | 6.87 | D | 95 | 5 | | 30 | | 50 | 5 | | |
| 1223 | A | 1 | H | 5 | 132.0 | 7.32 | D | | 10 | 90 | 1 | | 6 | 0 | 10 | |
| 1223 | A | 2 | H | 1 | 8.0 | 7.78 | D | 100 | | | | | | | contains highly birefringent fibrous mineral | |
| 1223 | A | 2 | H | 1 | 17.0 | 7.87 | D | 5 | | 95 | | 1 | | | | |
| 1223 | A | 2 | H | 1 | 35.0 | 8.05 | D | 100 | | | 10 | 10 | 70 | | | |
| 1223 | A | 2 | H | 2 | 26.0 | 8.47 | D | 100 | | | 20 | | 80 | | glass fragments sub-rounded to sub-angular | |
| 1223 | A | 2 | H | 3 | 50.0 | 9.38 | D | 100 | | | 40 | | 60 | | | |
| 1223 | A | 3 | X | 2 | 138.0 | 15.56 | D | 90 | 10 | | 60 | | 40 | | | |
| 1223 | A | 4 | X | 2 | 18.0 | 23.27 | D | | 20 | 80 | 1 | 10 | | | | |
| 1223 | A | 6 | X | 4 | 4.0 | 37.47 | D | | 40 | 60 | 40 | 30 | | 1 | | |

Figure F10. Example of a thin section description form.

Label of thin section indicates: Leg-Site-Core-Section depth in section (# of thin section)

| | | | |
|-----------------------|---|--------------------|--------------------|
| THIN SECTION: | 200-1224D-1R-4 1-4 cm (38) | Unit: | OBSERVER(S): ML |
| ROCK NAME: | Plagioclase sparsely-phyric basalt | GRAIN SIZE: | Very fine grained |
| WHERE SAMPLED: | | | |
| TEXTURE: | Intergranular to subophitic; isotropic, equigranular, holocrystalline | | |

PRIMARY MINERALOGY

| Phenocrysts | Percent Present | Percent Original | Size (mm) | | | Approximate composition | Morphology | Comments |
|-----------------------------|-----------------|------------------|-----------|------|-----|-------------------------|--------------------|---|
| | | | min. | max. | av. | | | |
| <i>Plagioclase</i> | ~ 1-2 | ~ 1-2 | 0.4 | 3 | 0.8 | Bytownite | Euhedral, columnar | % An > 80 (2Va ~ 85). Fresh, with no signs of alteration. Presence of one anhedral crystal ~ 0.9 mm long. |
| Groundmass/matrix | | | | | | | | |
| <i>Groundmass</i> | ~ 60 | | 0.1 | 0.6 | 0.3 | pl, cpx, op | Hypidiomorphic | Anhedral pale yellow cpx (augite; 2Vg ~ 65) in intergranular to subophitic relationship with subhedral to euhedral pl. In some cases pl is skeletal and the space between its arms is filled by microlites of cpx and skeletal op. Interstitial euhedral to anhedral op indicates its late appearance as liquidus phase. Rare presence (< 1%) of bytownite (2Va ~ 90) microphenocrysts (size < 0.6 mm). |
| <i>Segregation vesicles</i> | ~ 25 | | | | | | | Dark brown to black. These vesicles are made up by acicular to skeletal pl, equant cpx and tiny elongated op (ilmenite?) in a devitrified glassy matrix. These vesicles represent late stage magmatic melt. The rapid cooling is responsible for the skeletal shape of pl and mt crystals. |

SECONDARY MINERALOGY

| | Percent | | Size (mm) | | | Replacing/filling | Morphology | Comments |
|--------------------------|---------|--|-----------|------|-----|-------------------|------------|---|
| | | | min. | max. | av. | | | |
| <i>Clay minerals</i> | ~ 5 | | | | | | | Possibly replace former volcanic glass. Brownish, found in segregation vesicles and in cavities. |
| Vesicles/cavities | | | | | | | | |
| <i>Cavities</i> | ~ 5-6 | | 0.4 | 2.8 | 1.1 | | Spherical | All the cavities are totally filled. The filling material can be 1) brownish clay minerals (< 1 %), 2) microlitic intergrowth of pl, cpx, elongated op (all with size < 0.1 mm) plus possibly glass and clay minerals (~ 10 %) or 3) aragonite plus microlitic material (~ 90 %). Aragonite is always present in the biggest cavities, whereas microlitic material is the only filling only in the smallest cavities. |
| <i>Vesicles</i> | ~ 1 | | | | | | | Aragonite. |

COMMENTS : - Microlitic intergrowth partially filling cavities is the same material of segregation vesicles and may represent late stage magmatic melt patches
Microphotos? Yes
LEGEND: ol = olivine; cpx = clinopyroxene; pl = plagioclase; op = Fe-Ti oxides; mt = magnetite

Figure F11. Magnetic moment for the x-, y-, and z-axes measured for an empty sample boat at the beginning of Leg 200. A. Prior to cleaning the sample boat. (Continued on next page.)

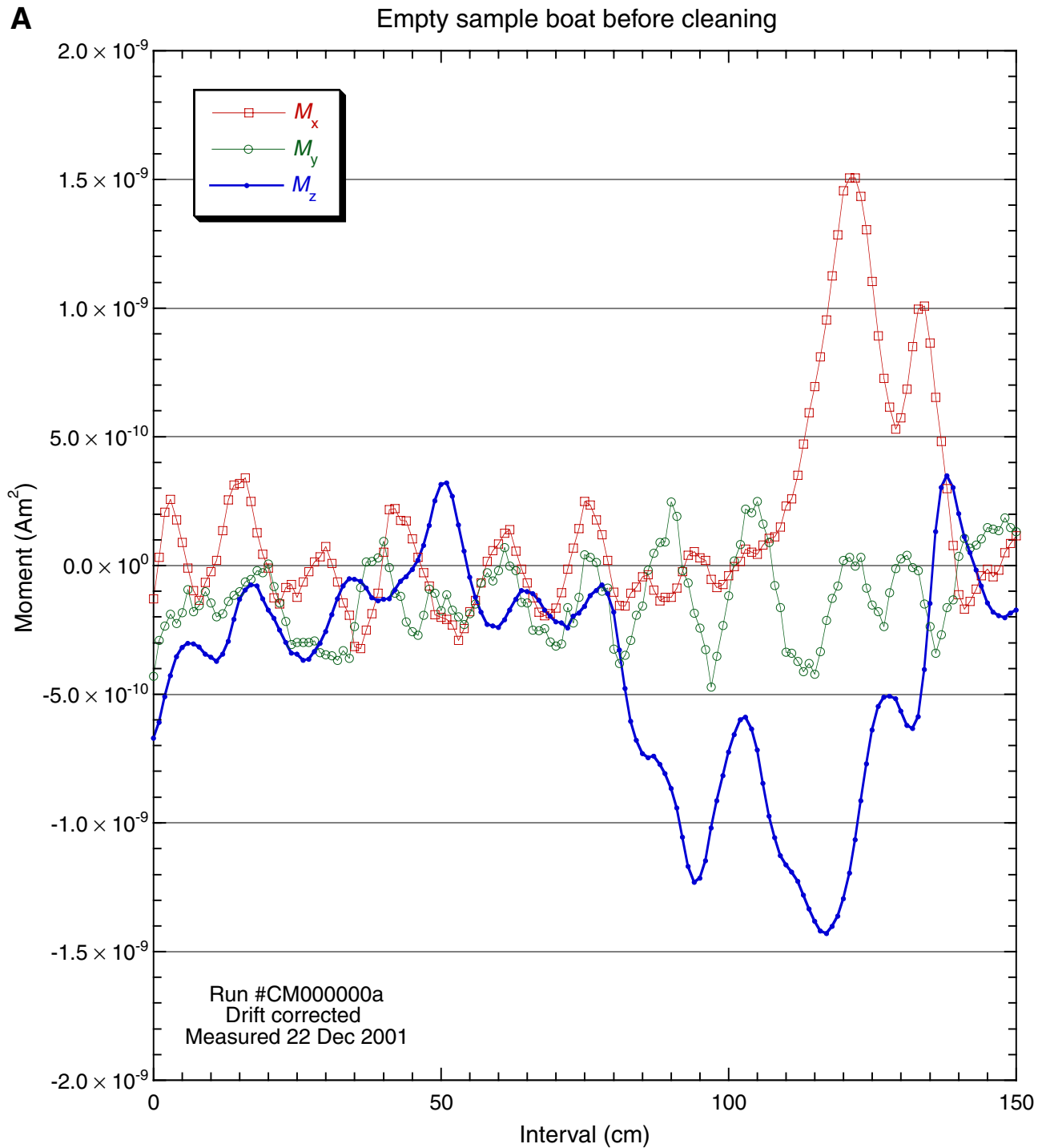


Figure F11 (continued). B. After the sample boat was cleaned with window cleaner and AF demagnetized at 60 mT.

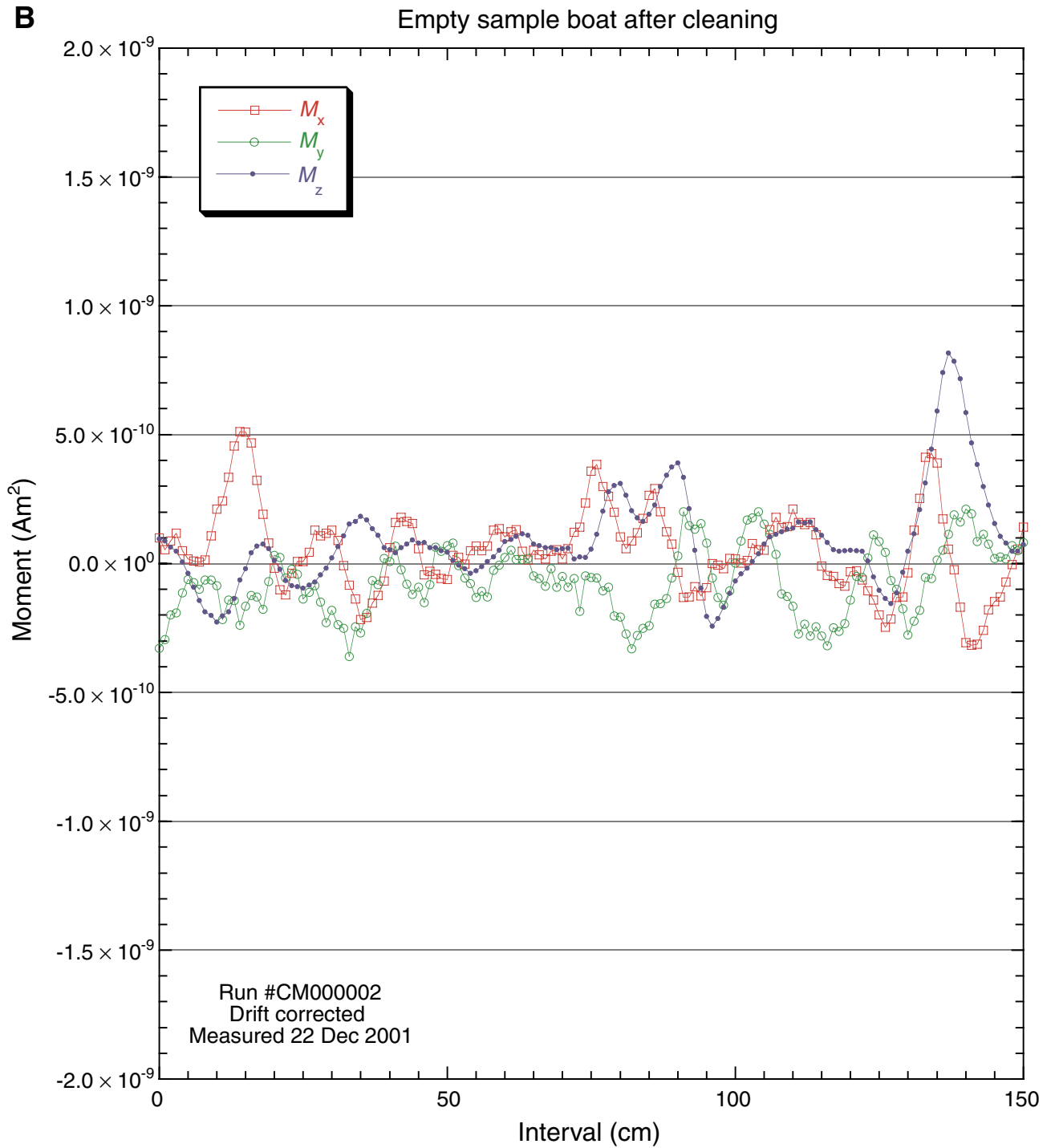


Figure F12. Magnetic moment for the x-, y-, and z-axes measured for an empty discrete sample tray sitting within the sample boat. The moment was measured along the 150-cm-long tray. A. Prior to cleaning. (Continued on next two pages.)

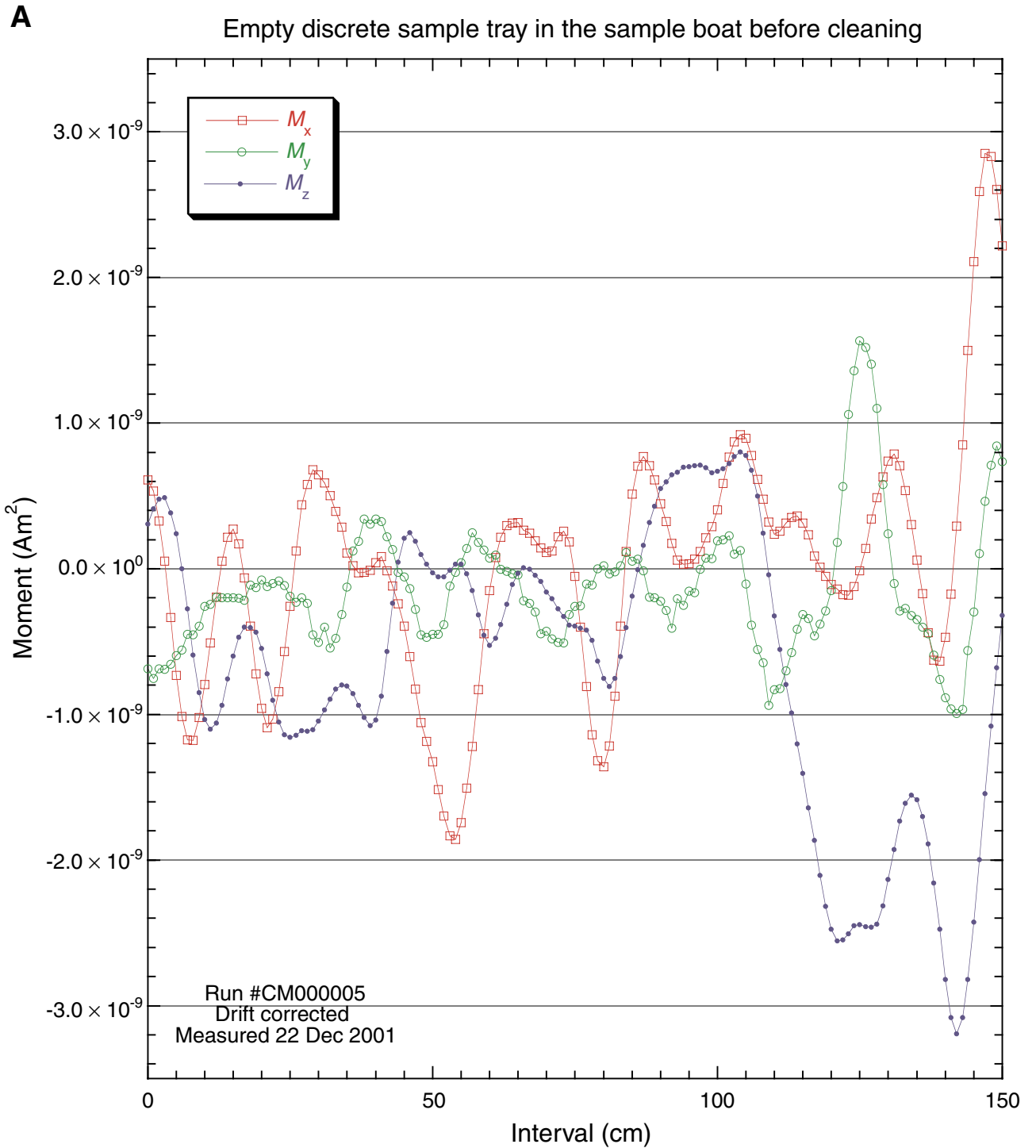


Figure F12 (continued). B. After the tray was cleaned with window cleaner and AF demagnetized at 60 mT.

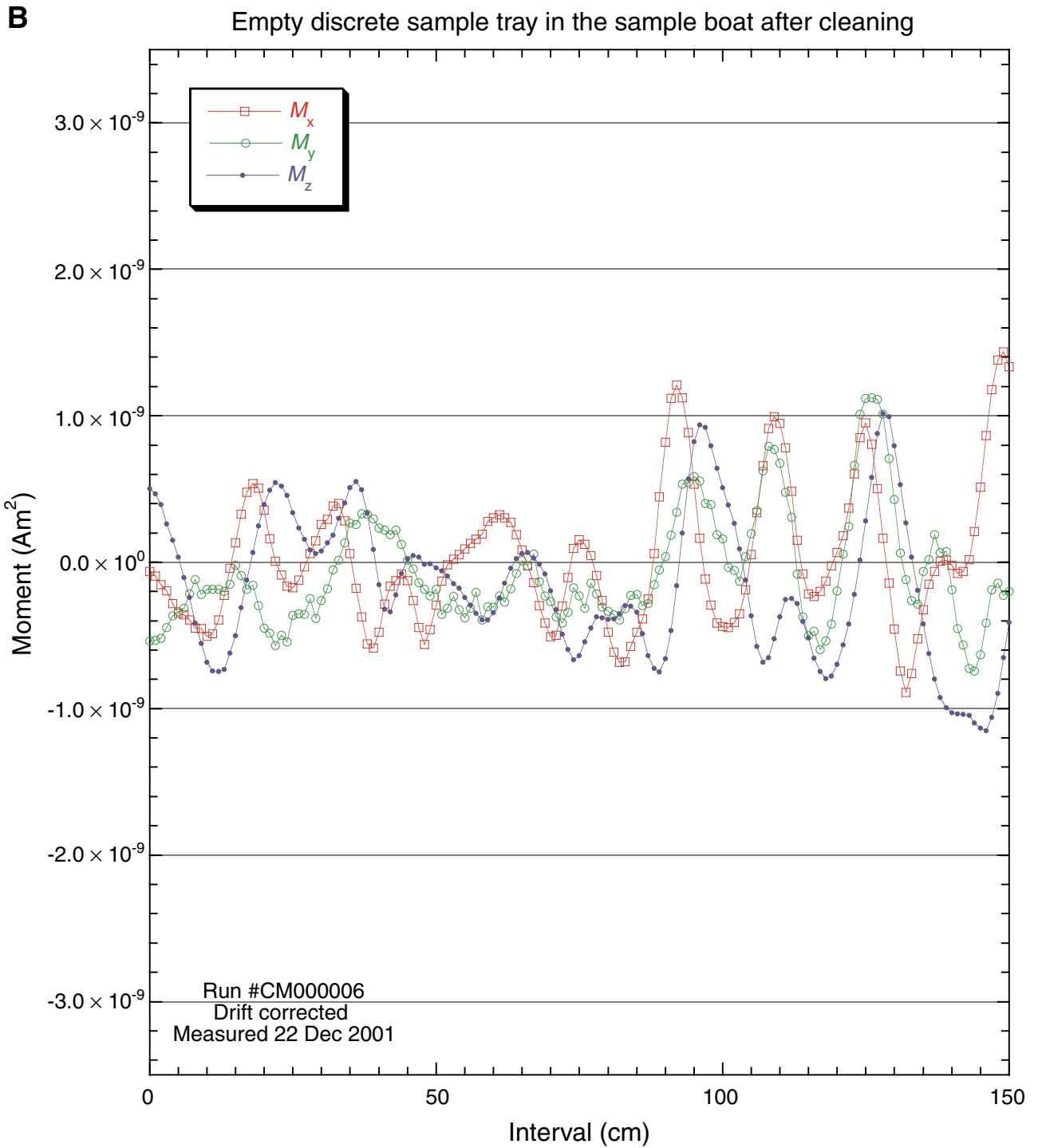


Figure F12 (continued). C. Several days later after the tray was cleaned and empty plastic cubes were inserted in the discrete sample holder positions.

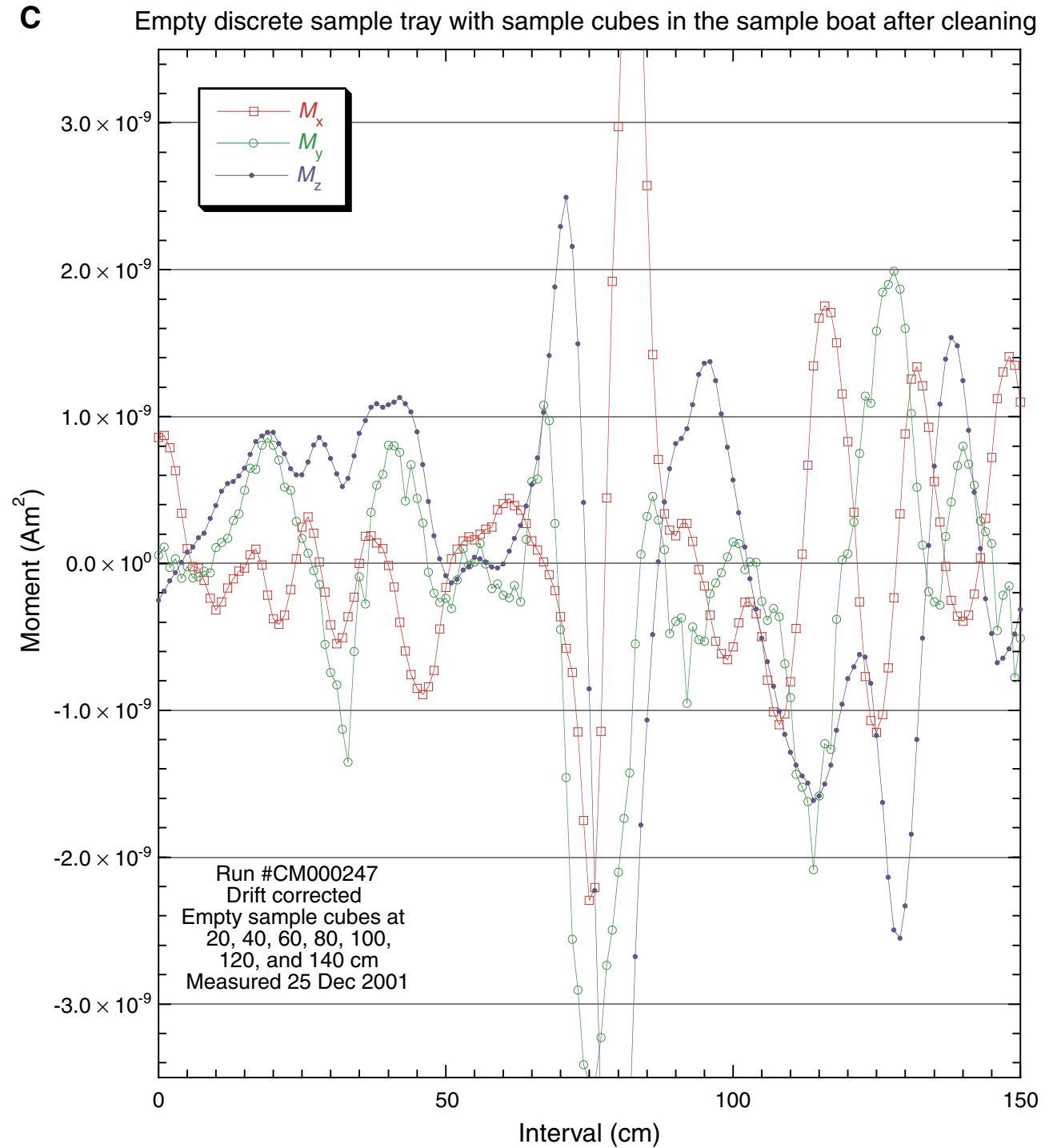


Figure F13. A. ODP paleomagnetic coordinate system for archive and working halves with radial and vertical overprints shown. B. Coordinate system for discrete samples collected with the extruder from the working half.

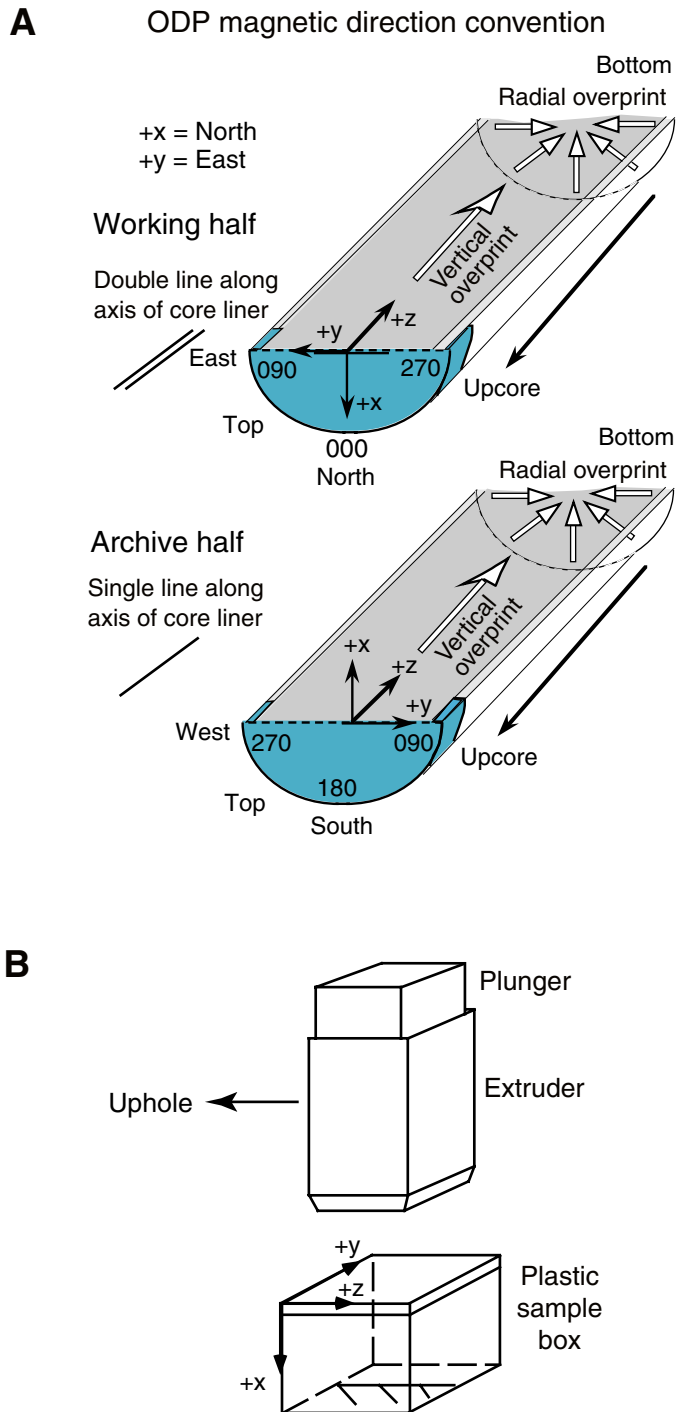


Figure F14. Schematic illustration of the configurations of tool strings run during Leg 200. SFLU = spherically focused log device, SP = spontaneous potential device.

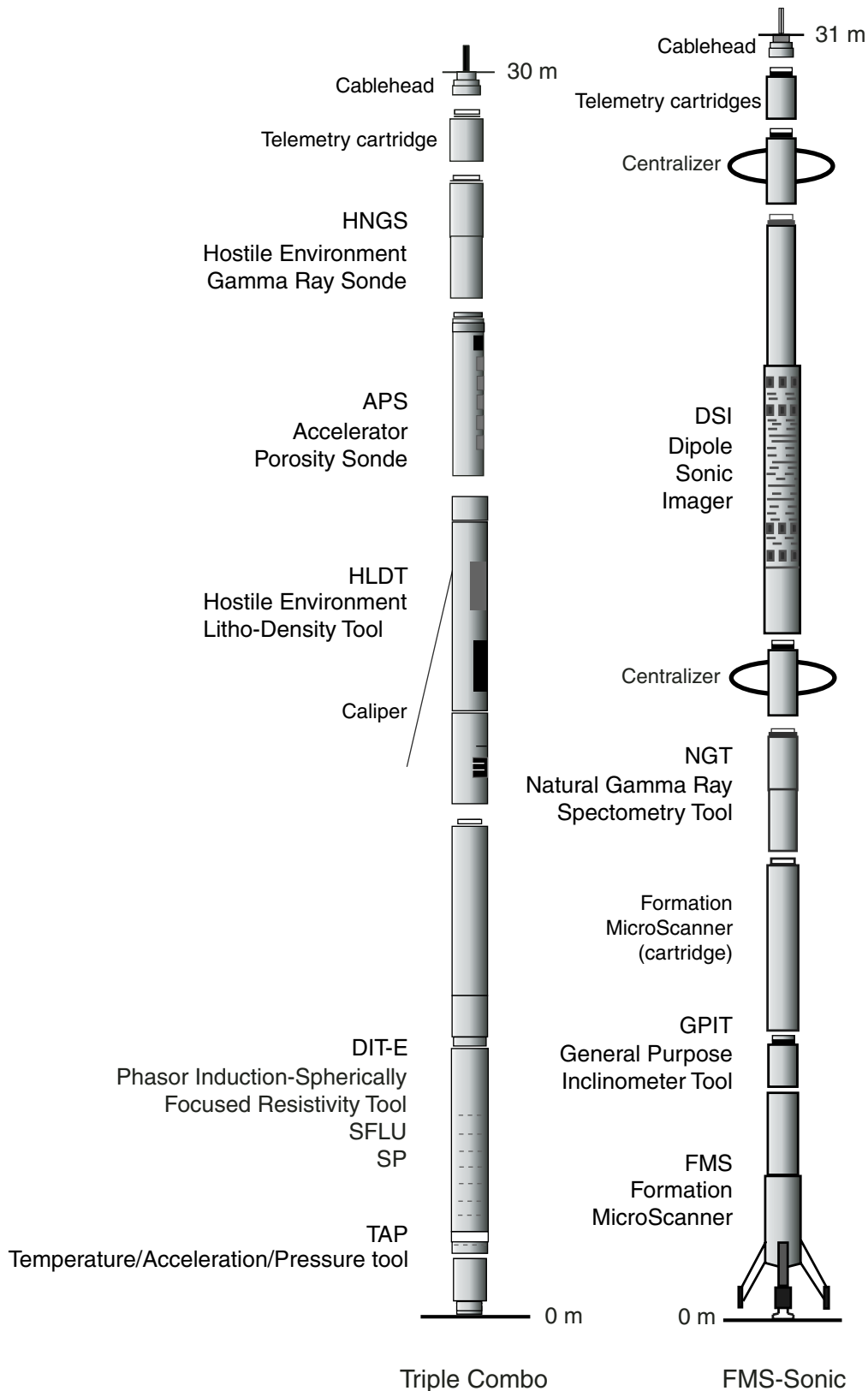
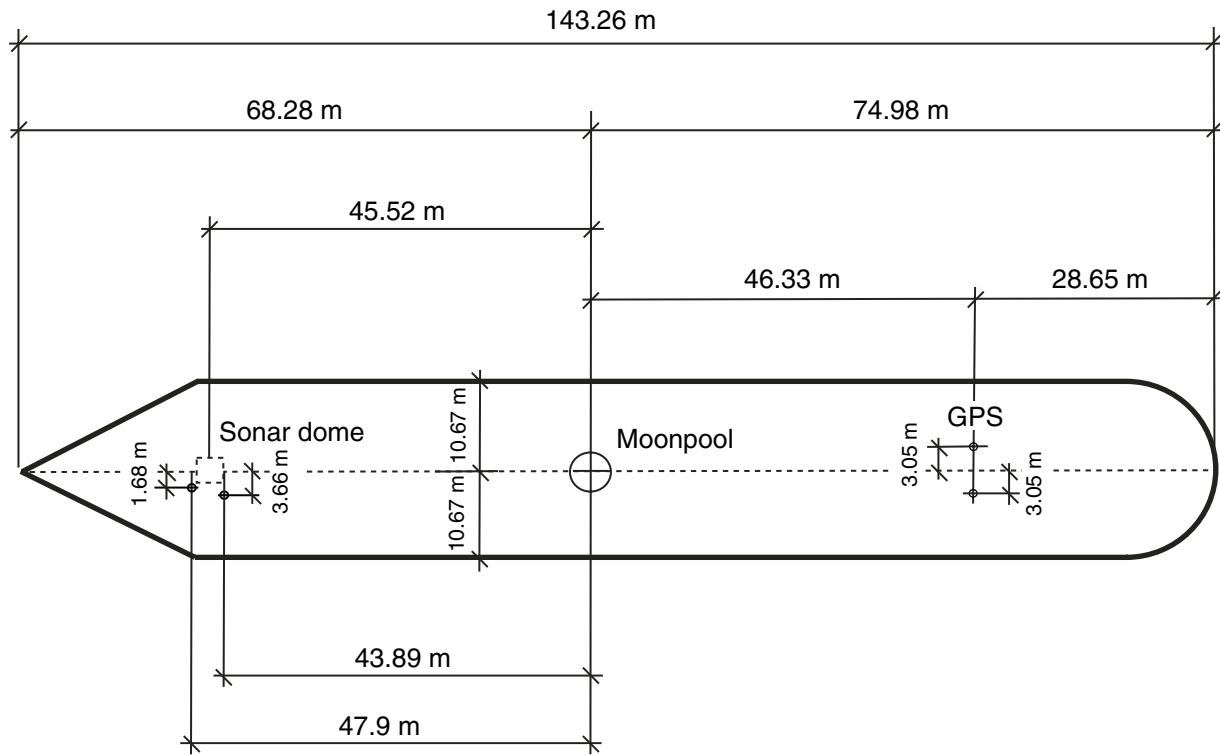


Figure F15. Summary of the significant dimensions necessary to correct the Global Positioning System (GPS) location of various antennas to the moonpool. (This figure was provided courtesy of the ODP under-way geophysics technicians.) fwd = forward, stb = starboard.



WinFrog ship configuration

Width of bow = 0.5 m
 Width of stern = 21.34 m

 Origin to bow = 68.28 m
 Origin to stern = 74.98 m
 Origin to bow curve = 45.52 m
 Origin to starboard side = 10.67 m
 Origin to port side = -10.67 m

Moonpool width = 5.0 m
 Moonpool fwd/aft = 0.0 m
 Moonpool port/stbd = 0.0 m

GPS antenna offset from origin
 Antenna fwd/aft = -46.33 m
 Antenna (OMNISTAR) port/stbd = 3.05 m
 Antenna (Ashtech) port/stbd = -3.05 m

Dynamic positioning GPS antennas

Trimble GPS antenna offset from origin
 Antenna fwd/aft = 47.9 m
 Antenna port/stbd = -1.68

Ashtech GPS antenna offset from origin
 Antenna fwd/aft = 43.89 m
 Antenna port/stbd = -3.66 m

Figure F16. Summary of the significant depth dimensions on the ship. The drillers commonly use the depth below the dual elevator stool (DES). The echo sounder depth corrected by Matthews' Tables gives the depth to the sonar dome. DP is the dynamic positioning control room. PDR refers to the depth from the precision depth recorder. (This figure was provided courtesy of the ODP underway geophysics technicians.)

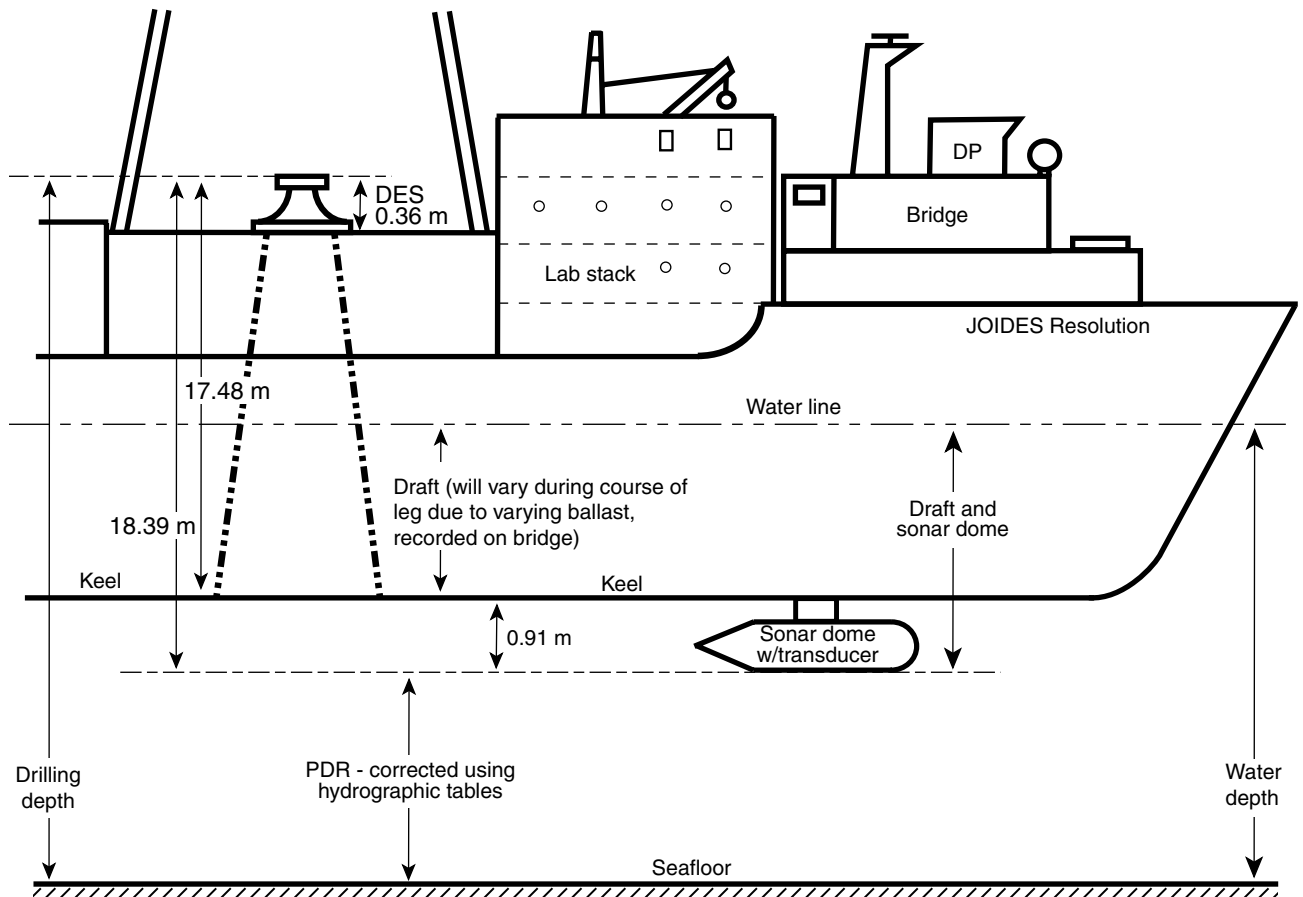


Figure F17. Summary of the significant depths and ranges for the single-channel seismic acquisition system and magnetometer system aboard the *JOIDES Resolution*. (This figure was provided courtesy of the ODP underway geophysics technicians.) GPS = Global Positioning System.

WinFrog streamer vehicle offset

80-in³ water gun = 193.5 m
 200-in³ water gun = 208.3 m
 Streamer drum circumference = 3.213 m
 47 wraps = ~150 m = optimal length to achieve equal gun and streamer depth

Single-channel hydrophone array

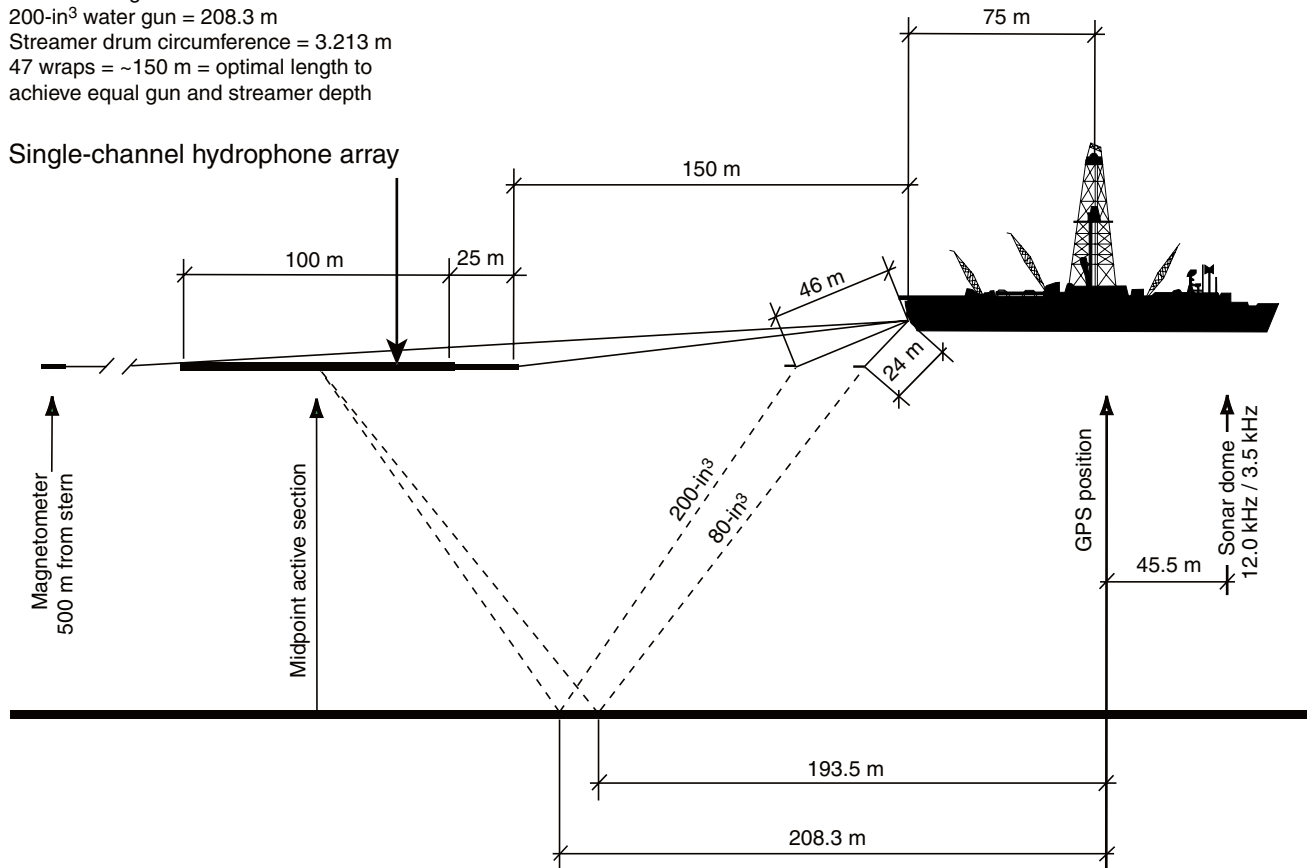


Figure F18. On the VIT frame, the 4.252-kHz transducer is the squat cylinder in the middle under the frame's horizontal member. The pinger batteries and electronics are in the cylinder to the upper left marked "Pinger."

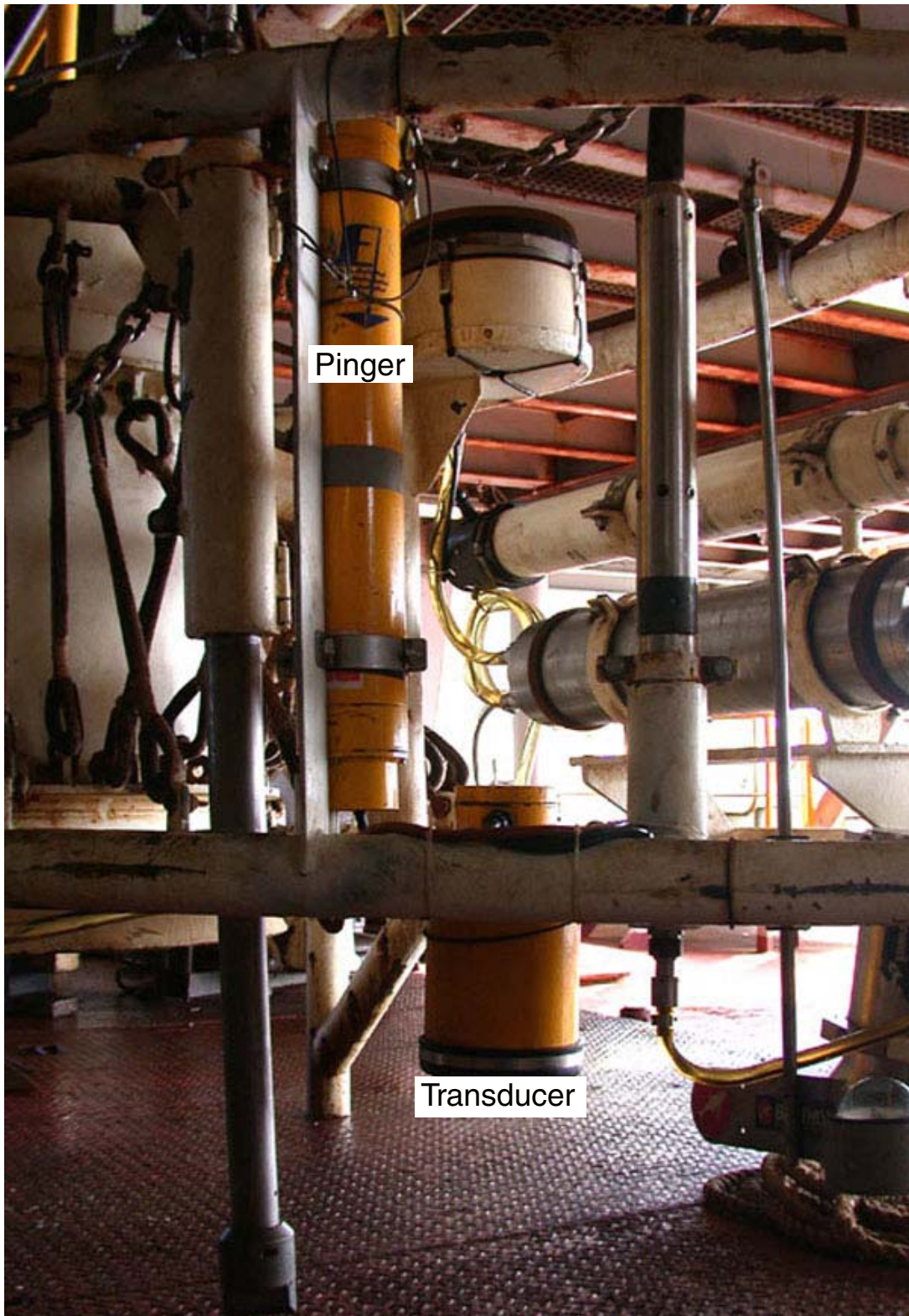


Table T1. ICP-AES analysis parameters used during Leg 200.

| Element | Instrument detection limit (ppb) | Wavelength (nm) | Slit width (nm)* | Integration time per calculation point (s) | Voltage (V) | Mode | Increment between points (nm)† | Calculation (pts) |
|---------|----------------------------------|-----------------|------------------|--|-------------|------|--------------------------------|-------------------|
| Al | 2.8 | 396.152 | 20/15 | 0.5 | 690 | 2 | 0.0020 | 5 |
| Ca | 0.2 | 393.366 | 20/15 | 0.5 | 330 | 2 | 0.0020 | 5 |
| Fe | 6.2 | 259.940 | 20/15 | 0.5 | 660 | 5 | 0.0020 | 5 |
| K | 60 | 766.490 | 20/15 Alk | 0.5 | 990 | 2 | 0.0020 | 5 |
| Mg | 1.6 | 285.213 | 20/15 | 0.5 | 730 | 5 | 0.0020 | 5 |
| Mn | 1.4 | 257.610 | 20/15 | 0.5 | 670 | 5 | 0.0020 | 5 |
| Na | 69 | 589.592 | 20/15 Alk | 0.5 | 590 | 2 | 0.0020 | 5 |
| P | 272 | 178.229 | 20/15 | 0.5 | 990 | 2 | 0.0020 | 5 |
| Si | 12 | 251.611 | 20/15 | 0.5 | 680 | 2 | 0.0020 | 5 |
| Ti | 3.8 | 334.941 | 20/15 | 0.5 | 730 | 2 | 0.0020 | 5 |
| Ba | 1.3 | 455.403 | 20/15 | 0.5 | 600 | 5 | 0.0020 | 5 |
| Cr | 7 | 267.716 | 20/15 | 0.5 | 680 | 5 | 0.0020 | 5 |
| Cu | 5.4 | 324.754 | 20/15 | 0.5 | 670 | 2 | 0.0020 | 5 |
| Ni | 15 | 231.604 | 20/15 | 0.5 | 780 | 2 | 0.0020 | 5 |
| Sc | 1.5 | 361.384 | 20/15 | 0.5 | 550 | 5 | 0.0020 | 5 |
| Sr | 0.4 | 407.771 | 20/15 | 0.5 | 780 | 2 | 0.0020 | 5 |
| V | 7.5 | 292.402 | 20/15 | 0.5 | 780 | 5 | 0.0020 | 5 |
| Y | 3.5 | 371.029 | 20/15 | 0.5 | 550 | 5 | 0.0020 | 5 |
| Zn | 1.8 | 213.856 | 20/15 | 0.5 | 810 | 2 | 0.0020 | 5 |
| Zr | 71 | 343.823 | 20/15 | 0.5 | 560 | 2 | 0.0020 | 5 |

Notes: BAS192 method acquisition parameters. * = widths of the entrance and exit slits; Alk = increase in sheath gas flow from 0.15–0.2 L/min to 0.8 L/min for analysis of these elements. † = interval between each of the calculation points in Mode 2, or the calculation window that constitutes the single point in Mode 5.

Table T2. Typical values for USGS standards analyzed by ICP-AES during Leg 200.

| | BHVO-2 | | | | BCR-2 | | | | BIR-1 | | | |
|--------------------------------|-------------|-------------|---------|-----------------|-------------|-------------|---------|-----------------|-------------|-------------|---------|-----------------|
| | 14 Jan 2002 | 17 Jan 2002 | Average | Certified value | 14 Jan 2002 | 17 Jan 2002 | Average | Certified value | 14 Jan 2002 | 17 Jan 2002 | Average | Certified value |
| Major element oxide (wt%): | | | | | | | | | | | | |
| SiO ₂ | 49.42 | 49.35 | 49.39 | 49.85 | 54.23 | 54.31 | 54.27 | 54.10 | 48.05 | 48.07 | 48.06 | 47.77 |
| TiO ₂ | 2.77 | 2.66 | 2.72 | 2.69 | 2.20 | 2.31 | 2.26 | 2.26 | 0.99 | 1.01 | 1.00 | 0.96 |
| Al ₂ O ₃ | 13.58 | 13.53 | 13.56 | 13.85 | 12.82 | 13.39 | 13.1 | 13.50 | 15.84 | 15.45 | 15.65 | 15.35 |
| Fe ₂ O ₃ | 12.35 | 12.19 | 12.27 | 12.23 | 13.79 | 13.86 | 13.8 | 13.80 | 11.29 | 11.34 | 11.32 | 11.26 |
| MnO | 0.19 | 0.19 | 0.19 | 0.17 | 0.23 | 0.23 | 0.23 | 0.24 | 0.20 | 0.20 | 0.20 | 0.171 |
| MgO | 7.17 | 7.20 | 7.19 | 7.31 | 3.56 | 3.57 | 3.57 | 3.59 | 9.74 | 9.71 | 9.72 | 9.68 |
| CaO | 11.35 | 11.18 | 11.27 | 11.33 | 7.09 | 7.22 | 7.16 | 7.12 | 13.39 | 13.24 | 13.32 | 13.24 |
| Na ₂ O | 2.22 | 2.23 | 2.23 | 2.29 | 3.11 | 3.13 | 3.12 | 3.16 | 1.84 | 1.80 | 1.82 | 1.75 |
| K ₂ O | 0.55 | 0.54 | 0.55 | 0.54 | 1.78 | 1.82 | 1.80 | 1.79 | 0.010 | 0.015 | 0.01 | 0.027 |
| P ₂ O ₅ | 0.27 | 0.26 | 0.27 | 0.27 | 0.35 | 0.35 | 0.35 | 0.35 | 0.047 | 0.055 | 0.05 | 0.046 |
| Totals: | 99.87 | 99.33 | 99.64 | 100.53 | 99.16 | 100.19 | 99.66 | 99.91 | 101.40 | 100.89 | 101.17 | 100.25 |
| Trace element (ppm): | | | | | | | | | | | | |
| Ni | 113 | 98 | 106 | 119 | 23 | 23 | 23 | 20 | 168 | 150 | 159 | 166 |
| Cr | 275 | 281 | 278 | 280 | 16 | 13 | 15 | 18 | 386 | 382 | 384 | 382 |
| V | 316 | 315 | 316 | 317 | 416 | 416 | 416 | 416 | 314 | 316 | 315 | 313 |
| Zr | 169 | 173 | 171 | 172 | 191 | 187 | 189 | 188 | 13 | 16 | 15 | 16 |
| Sc | 32 | 34 | 33 | 32 | 34 | 33 | 34 | 33 | 44 | 41 | 43 | 44 |
| Y | 26 | 27 | 27 | 26 | 37 | 37 | 37 | 37 | 16 | 16 | 16 | 16 |
| Sr | 396 | 393 | 395 | 389 | 338 | 346 | 342 | 346 | 109 | 110 | 110 | 108 |
| Ba | 129 | 134 | 132 | 130 | 683 | 682 | 683 | 683 | 8 | 10 | 9 | 7 |

Notes: Iron is represented as Fe³⁺. Certified values were used as concentrations in calculating regressions.

Table T3. Logging tool and measurement units and acronyms.

| Tool string | Tool | Output | Explanation | Units |
|-----------------------------------|-------|---|---|--|
| Triple combination | APS | APLC | Accelerator porosity sonde | |
| | | FPLC | Near array porosity (limestone calibrated) | Fraction |
| | | SIGF | Far array porosity (limestone corrected) | Fraction |
| | | STOF | Formation capture cross section (Σ_i) | Capture units |
| | | STOF | Tool standoff (computed distance from borehole wall) | in |
| | DIT | | Dual induction tool | |
| | DIT-E | | Phasor induction-spherically focused resistivity tool | |
| | | IDPH | Deep induction resistivity | Ωm |
| | | IMPH | Medium induction resistivity | Ωm |
| | | SFLU | Spherically focused resistivity | Ωm |
| | | SP | Spontaneous potential | mV |
| | HLDT | | Hostile environment litho-density tool | |
| | | RHOB | Bulk density (corrected) | g/cm^3 |
| | | PEF | Photoelectric effect | b/e^- |
| | | CALI | Caliper (measure of borehole diameter) | in |
| | | DRHO | Bulk density correction | g/cm^3 |
| | HNGS | | Hostile environment gamma ray sonde | |
| | | HSGR | Standard (total) gamma ray | gAPI |
| | | HCGR | Computed gamma ray (HSGR minus uranium contribution) | gAPI |
| | | HFK | Potassium | Fractional % |
| | HTHO | Thorium | ppm | |
| | HURA | Uranium | ppm | |
| | TAP | | Temperature/acceleration/pressure tool | $^{\circ}\text{C}$, m/s^2 , psi |
| Formation MicroScanner/Sonic | DSI | | Dipole sonic imager | |
| | | DTCO | Compressional wave delay time (Δt) | ms/ft |
| | | DTSM | Shear wave delay time (Δt) | ms/ft |
| | | DTST | Stoneley wave delay time (Δt) | ms/ft |
| | FMS | | Formation MicroScanner | |
| | | | Oriented images of borehole microductance | |
| | GPIT | | General purpose inclinometer tool | |
| | | F_x, F_y, F_z | Earth's magnetic field (three orthogonal components) | Degrees |
| | | A_x, A_y, A_z | Acceleration (three orthogonal components) | m/s^2 |
| | NGT | | Natural gamma ray spectrometry tool | |
| | SGR | Standard total gamma ray | gAPI | |
| | CGR | Computed gamma ray (SGR minus uranium contribution) | gAPI | |
| | POTA | Potassium | % | |
| | THOR | Thorium | ppm | |
| | URAN | Uranium | ppm | |
| Three-component Well Seismic Tool | WST | | Well seismic tool | |
| | | | Acoustic arrival times | ms |

Table T4. Leg 200 logging tool specifications.

| Tool string* | Tool† | Measurement | Sampling interval (cm) | Approximate vertical resolution (cm) | Approximate depth of investigation (cm) |
|---------------------------------|-------|--|------------------------|--------------------------------------|---|
| Triple combination | HNGS | Natural gamma ray | 15 | 45 | Variable |
| | APS | Porosity | 5 and 15 | 30 | 15 |
| | HLDS | Bulk density, PEF | 15 | 38 | 15 |
| | DIT-E | Resistivity | 15 | 150/90/60 | 150/76/38 |
| | TAP | Temperature/ Acceleration/ Pressure tool | 1/s 4/s 1/s | | |
| Formation MicroScanner/Sonic | FMS | Resistivity image | 0.25 | 0.5 | 15 |
| | NGT | Natural gamma ray | 15 | 45 | 45 |
| | GPIT | Tool orientation | 1 or 15 | NA | NA |
| | DSI | Sonic velocity | 15 | 110 | 15–30 |

Notes: * = all tool and tool string names (except the TAP tool) are trademarks of Schlumberger. † = for additional information about tool physics and use consult ODP Logging Services at www.ldeo.columbia.edu/BRG/ODP. PEF = photoelectric effect factor. See Table T3, p. 64, for explanations of acronyms used to describe tool strings and tools. NA = not applicable.

Table T5. WST-3 tool specifications.

| Axis | Three axis |
|----------------------------|---|
| Geophones | One per axis |
| Geophone frequency | 10 Hz |
| Sampling rate | 1, 2, or 4 ms (selectable) |
| Low-cut frequency | 0.2 Hz |
| Low-cut slope | 18 dB/octave |
| High-cut frequency | 250 Hz for 1-ms sampling 125 Hz for 2- and 4-ms sampling |
| High-cut slope | 36 dB/octave |
| Digitalization | Downhole |
| ADC resolution | 11 bit + sign |
| Autoranger steps | Five 6-dB steps |
| Preamplifier gain | 40 to 106 dB by 6-dB steps for each axis |
| Dynamic range per waveform | 90 dB |
| Total dynamic range | 156 dB |

Note: ADC = analog to digital converter.